High-Resolution 17 O Solid-State NMR as a Unique Probe for Investigating Oxalate Binding Modes in Materials: The Case Study of Calcium Oxalate Biominerals

Ieva Goldberga, Ivan Hung, Vincent Sarou-Kanian, Christel Gervais, Zhehong Gan, Jessica Novák-Špačková, Thomas-Xavier Métro, César Leroy, Dorothée Berthomieu, Arie van der Lee, et al.

HAL Id: hal-04603458

https://hal.umontpellier.fr/hal-04603458v1

Submitted on 29 Oct 2024

High-resolution ^{17}O solid-state NMR as a unique probe for investigating oxalate binding modes in materials: The case study of calcium oxalate biominerals

Ieva Goldberga,[1,a,*] Ivan Hung,[2] Vincent Sarou-Kanian,[3] Christel Gervais,[4,*] Zhehong Gan,[2] Jessica Novák-Špačková,[1,b] Thomas-Xavier Métro,[1] César Leroy,[1] Dorothée Berthomieu,[1] Arie van der Lee,[5] Christian Bonhomme,[4] Danielle Laurencin[1,*]

[1] ICGM, Univ Montpellier, CNRS, ENSCM, 34293 Montpellier, France

[2] National High Magnetic Laboratory (NHMFL), Tallahassee, Florida, 32310, USA

[3] CNRS, CEMHTI UPR3079, Université d'Orléans, 45071 Orléans, France

[4] LCMCP, UMR 7574, Sorbonne Université, CNRS, 75005 Paris, France

[5] IEM, Univ Montpellier, CNRS, ENSCM, 34095 Montpellier, France

[a]Current affiliation: LCMCP, UMR 7574, Sorbonne Université, CNRS, 75005 Paris, France

[b]Current affiliation: Synthon, 67801 Blansko, Czech Republic

[*]To whom correspondence should be addressed:

ieva.goldberga@sorbonne-universite.fr

christel.gervais_stary@sorbonne-universite.fr

danielle.laurencin@umontpellier.fr

Abstract

Oxalate ligands are found in many classes of materials, including energy-storage materials and biominerals. Determining their local environments at the atomic scale is thus paramount to establishing the structure and properties of numerous phases. Here, we show that high-resolution ^{17}O solid-state NMR is a valuable asset for investigating the structure of crystalline oxalate systems. First, an efficient [17]O-enrichment procedure of oxalate ligands is demonstrated using mechanochemistry. Then, [17]O-enriched oxalates were used for the synthesis of the biologically relevant calcium-oxalate monohydrate (COM) phase, enabling the analysis of its structure and heat-induced phase transitions by high-resolution ^{17}O NMR. Studies of the low-temperature COM form (LT-COM), using magnetic fields from 9.4 to 35.2 T, as well as [13]C-[17]O MQ/D-RINEPT and [17]O{[1]H} MQ/REDOR experiments, enabled the 8 inequivalent oxygen sites of the oxalates to be resolved, and tentatively assigned. The structural changes upon heat treatment of COM were also followed by high-resolution ^{17}O NMR, providing new insight into the structures of the high-temperature form (HT-COM) and anhydrous calcium oxalate α-phase (α-COA), including the presence of structural disorder in the latter case. Overall, this work highlights the ease associated with [17]O-enrichment of oxalate oxygens, and how it enables high-resolution solid-state NMR, for "NMR-crystallography" investigations.

TOC
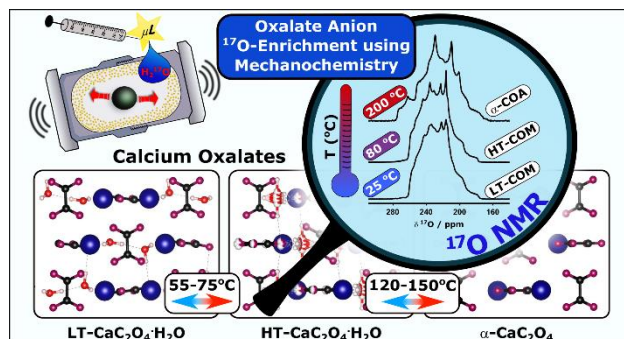
Synopsis text

Oxalate ligands are found in many classes of materials. Determining their local environments at the atomic scale is thus key to establishing the structure and properties of numerous phases. Here, we show that high-resolution 17O NMR is a valuable asset for studying crystalline oxalate systems. Using advanced [17]O labeling schemes, high resolution ^{17}O ssNMR experiments (including at different magnetic fields and temperatures), and computational modeling, new structural insight on Ca-oxalate biominerals can be reached.

Introduction

Oxalate anions are found in numerous molecules and materials across various disciplines, including geology, life and (nano)materials sciences. The small size and many different coordination modes of oxalate ligands towards metal centers explains the wide diversity of metal oxalate structures. Numerous studies have been carried out on transition metal oxalates, showing that they can be attractive as energy storage materials for CO_2 capture, or as interesting components for Li, Na-ion and redox batteries.[1] Furthermore, synthetic coordination networks containing oxalate anions have been widely investigated,[2,3] with luminescent properties in the case of lanthanum-based metal-organic frameworks (MOFs),[4] and magnetic properties for transition metal and lanthanide oxalates.[5–7] In the nuclear industry, oxalate ions are also used as a precipitating agent for purification and isolation purposes of actinides, which are further decomposed to obtain the corresponding oxides.[8] In Nature, there are over 20 minerals reported to contain oxalate ions,[9] chelating various cations found in soil and plants such as alkaline earth metals, transition metals, and rare earth elements.[10–12]

Calcium oxalate minerals are associated with pathological biomineralization processes in humans, leading to kidney stone disease (urolithiasis).[13–15] Notably, the monohydrate form ($CaC_2O_4 \cdot H_2O$, whewellite, COM) is the predominant phase in kidney stones.[15,16] Depending upon the temperature, whewellite can adopt two structures – so-called low and high-temperature forms (denoted as LT and HT, respectively) (Figure 1). Upon further heat treatment (up to ~410 °C), several anhydrous polymorphs can also be obtained synthetically (CaC_2O_4, noted COA),[17,18] which are unstable under ambient laboratory conditions and rehydrate back to the COM.[18,19] The transitions between these phases lead to changes in lattice cell parameters and local environments of the oxalates (Figures S1 and S2), with notably increased dynamics around the neighboring water molecules in the HT-COM, and variations in the distances to neighboring calcium cations.[17,20]
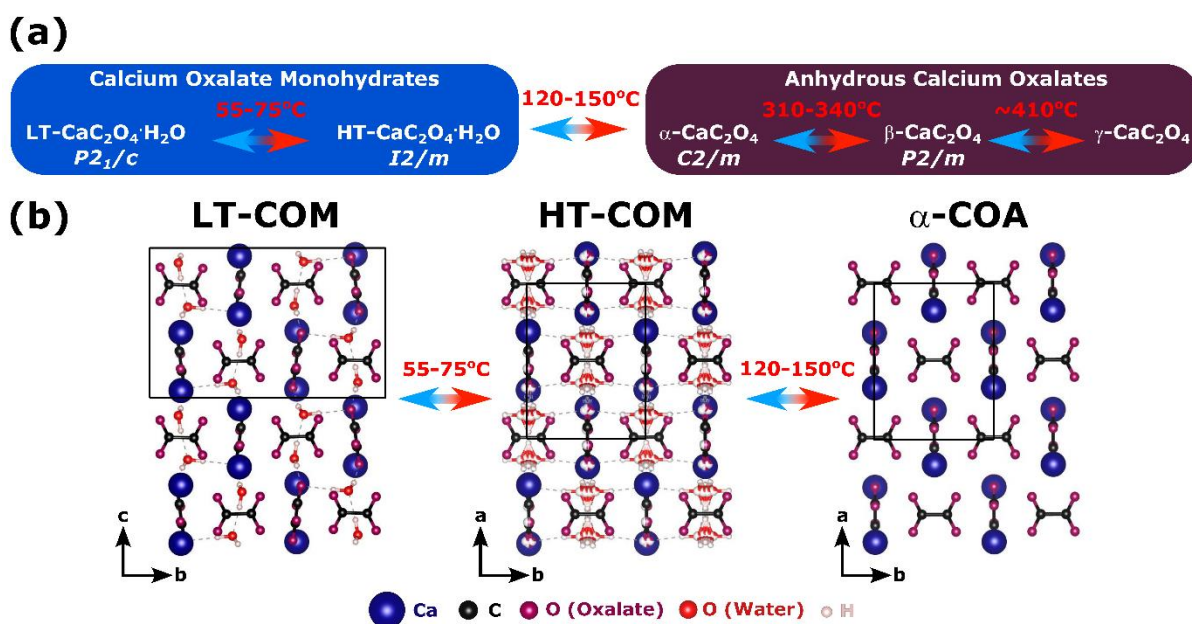
Figure 1. (a) Chemical and structural evolution of calcium oxalates upon heat treatment (as proposed by Izatulina *et al*).[17] (b) Structural relationships between LT-COM, HT-COM and α-COA. Note that the reported *I*2/*m* symmetry for HT-COM is equivalent to *C*2/*m* symmetry by a cell transformation and that the dehydration from HT-COM to α-COA is an isostructural process.

Due to the prevalence of oxalate anions in a wide variety of natural and synthetic structures, detailed studies of their local environment within materials like those mentioned above are essential. A precise description of their coordination modes can give insights into their chemical and physical properties. Such structural studies can be carried out using a wide range of analytical techniques, like infrared (IR) and Raman spectroscopies, solid-state Nuclear Magnetic Resonance (ssNMR), and X-ray diffraction (XRD) (for crystalline phases). Despite their usefulness, each of these techniques has its shortcomings. IR and Raman studies can give information on the coordination of oxalate ions,[21–23] but cannot always differentiate between different polymorphs.[24] Powder and single crystal XRD analysis can provide more structural information,[4,25] including polymorphism;[17] but is unsuitable for studying amorphous materials. Regarding ssNMR, studies on oxalate-containing materials have been carried out at natural abundance on the ^{13}C nucleus,[26,27] but have required isotopic enrichment for ^{17}O, due to its much lower natural abundance (~ 0.037% for ^{17}O, *vs* ~ 1.1% for ^{13}C).[28,29] As oxygen is directly involved in the binding to the metal centers, ^{17}O ssNMR is a promising probe for structural studies, especially when considering that the chemical shift range for carboxylate oxygens spans over 50 ppm (from ≈ 250 to 300 ppm).[30–32] Furthermore, DFT calculations have shown that the isotropic chemical shift (δ_{iso}) of oxalate oxygens is sensitive to the bonding strength of oxalate ion to the metal centre.[31] However, in addition to poor sensitivity, ^{17}O ssNMR also suffers from poor spectral resolution due to the quadrupolar

nature of the oxygen-17 (spin-5/2) nuclide, and isotopic enrichment is thus essential to carry out high-resolution analyses.

For calcium oxalates, the transformations between the different forms presented in Figure 1 have been investigated so far by XRD,[17,18,33] IR and Raman spectroscopies,[24,34] as well as thermogravimetric analysis (TGA), scanning electron microscopy (SEM), or differential scanning calorimetry (DSC) techniques.[33,35] Moreover, multinuclear ssNMR analyses have been carried out, showing that the changes in the oxalate local environment upon reversible transition of COM from the LT to the HT form can be followed by ^{13}C NMR,[26] and that the variations in dynamics of the water molecules during the same transformation can be investigated using ^{17}O and ^{2}H ssNMR (after isotopic enrichment of water with [17]O or ^{2}H).[36] Yet, to the best of our knowledge, no method has been proposed to probe directly the binding of the oxalate ligand oxygen atoms to its neighbors (*i.e.*, calcium ions through coordination bonds, and protons of water molecules through hydrogen bonding). While ^{17}O ssNMR naturally appears as a promising method for studying oxalate oxygens, the enrichment procedures currently described in the literature (isotopic exchange starting from oxalic acid or sodium oxalate) involve up to 1 mL of [17]O-enriched water,[28,29,37] which can be particularly expensive and not optimal for subsequent syntheses of oxalate-based (nano)materials, considering the high cost of [17]O-labeled water (1800 – 2900 EUR for 1 mL of 90% oxygen-17 enriched H_2O, as of publication date). Based on our recent developments of [17]O-labeling protocols for carboxylic groups using mechanochemistry, which enabled the efficient labeling of fatty acids and amino acids using only microliter quantities of $H_2^{17}O$,[38–40] we decided *(i)* to test this enrichment methodology to the label oxalate oxygen atoms, and *(ii)* to demonstrate how such labeled ligands can then be used to probe *via* advanced ^{17}O ssNMR analyses the structure and reactivity of biominerals involved in pathological calcifications.

This article describes high-resolution ^{13}C and ^{17}O ssNMR studies of the LT-COM, HT-COM and COA forms, including *in situ* variable-temperature investigations to monitor the changes occurring upon heat treatment. It will be shown that ^{17}O ssNMR analyses of oxalate binding provide highly complementary information compared to ^{13}C ssNMR, and can lead to valuable insights into the different phase transformations, further emphasizing that this technique can be valuable for the study of other oxalate systems.

Experimental section

Reagents

Dimethyl oxalate ($C_4H_6O_4$, 99%, Alfa Aesar), diethyl oxalate ($C_6H_{10}O_4$, 99%, Sigma-Aldrich), diethyl oxalate-$^{13}C_2$ ($(C_2H_5O_2{}^{13}C)_2$, 99 atom % ^{13}C, Sigma-Aldrich), calcium chloride dihydrate ($CaCl_2\cdot2H_2O$, 99%, Sigma-Aldrich), $H_2{}^{17}O$ (~40% or ~90% ^{17}O enrichment, CortecNet), $H_2{}^{18}O$ (99.3% ^{18}O enrichment, CortecNet) and sodium ethoxide (NaOEt, >95%, Sigma-Aldrich) were used as received. HPLC-grade water (Acros Organics) was used for work-up procedures and precipitation of COM.

Synthesis of isotopically-labeled COM: isotopic enrichment of oxalates

Preparation of ^{17}O-COM (and ^{18}O-COM)

The enrichment of oxalate oxygens was achieved through mechanochemical saponification of an ester-derivative of oxalic acid (Scheme 1), by adapting experimental procedures previously reported to prepare $^{17}O/^{18}O$-enriched fatty acids and amino acids.[38,40] The labeled hydroxy ions (H^*O^-) are produced *in situ* by reaction of EtONa with $H_2{}^*O$, and react with the ester derivative of the carboxylic acid. Ball-milling (BM) experiments were performed on a Retsch Mixer Mill MM400 apparatus, using milling jars and beads pre-dried under vacuum before the syntheses.

In a typical experiment, two stainless-steel beads (10 mm diameter) and a stainless-steel jar (inner volume 10 mL; screw-cap lid) were used. In the reactor, beads were introduced first, followed by dimethyl oxalate (134 mg, 1.13 mmol, 1.0 equiv), sodium ethoxide (190 mg, 2.80 mmol, 2.5 equiv) and isotopically enriched water (60.5 µL, 3.36 mmol, 3 equiv). The reactor was closed and sealed using parafilm, and reagents were subjected to grinding for 30 minutes at 25 Hz. ATR-IR analyses confirmed the completion of the saponification by the shift in the carbonyl stretching vibration band from ~1735 to ~1623 cm^{-1} (Figure S3). Then, HPLC grade water (1 mL) was added to the pasty, light beige reaction mixture. The jar was closed, sealed with parafilm, and further milled for 2 minutes at 25 Hz. The light beige solution was recovered and transferred to a conical flask. To ensure all product was retrieved, the milling jar was further washed with 4 mL of HPLC grade water and added to the conical flask. The pH of the solution was then adjusted to 6.5 – 7.0 using 1M HCl (~250 µL).

The volume of the solution (containing solvated $Na_2C_2{}^*O_4$) was then adjusted to reach a ~0.1 M concentration for the oxalate. Separately, a ~0.1 M aqueous solution of $CaCl_2$ was prepared. Both solutions (of equimolar concentrations) were then introduced in separate syringes (with a typical volume of ~11.1 mL), and added simultaneously with a syringe pump at a rate of 0.25 mL/ min in a round bottom flask, initially containing 1 mL of HPLC grade water, under magnetic stirring. The formation of a white precipitate was observed instantaneously. The reaction mixture was left under magnetic stirring for approximately one hour. The white solid was filtered and dried under vacuum at room temperature (~18 hours).

The final product (149 ± 2 mg) was found to be a mixture of calcium oxalate monohydrate (COM) and dihydrate (COD) phases, as shown by powder XRD (pXRD) and ATR-IR analyses (see Figures S4 (a) and S5 (a)). To obtain phase pure COM, the white solid was soaked in ~1.5 mL of HPLC-grade water in a 2 mL Eppendorf tube and left immersed for 72 hours at room temperature (without stirring). Excess water was removed by centrifugation at 20 000 rpm for 10 minutes, and the remaining solid was then dried under vacuum for six hours. In cases when traces of COD were still observed (by pXRD and ATR-IR analysis), the solid was subjected to further soaking in water and drying cycles until no dihydrate was detected by these two analytical techniques.

Preparation of ^{13}C-COM and ^{13}C/^{17}O-COM

The ^{13}C-enriched COM phase (^{13}C-COM) was prepared following a procedure analogous to the one described in the previous section. However, instead of dimethyl oxalate, diethyl oxalate-^{13}C$_2$ (150 ± 1 µL, 1.0 equiv) was used as a precursor to yield ^{13}C enrichment in oxalate carbon atoms, and HPLC grade water was used instead of enriched water in the saponification step. The fact that diethyloxalate is a liquid in ambient laboratory conditions (while dimethyloxalate is a solid) did not change the outcome of the reaction.

A doubly enriched COM phase (^{13}C/^{17}O-COM) was also prepared using diethyl oxalate-^{13}C$_2$ and H$_2$^{17}O (~90% ^{17}O).

For these syntheses, the white precipitate (typically obtained in quantities ~155 ± 3 mg after drying) was subjected to further soaking in water and drying cycles, as described in the previous section, to eventually lead to the formation of phase pure enriched COM samples (Figures S4 (b) and S5 (b)).

Storage of enriched COM phases

All phase pure COM samples were stored in parafilmed glass vials and placed in a container together with molecular sieves at -16 °C until further use. Prior to any characterization by IR, pXRD and ssNMR, samples were taken out of the freezer and left to thaw for 30 minutes.

Scheme 1. Top: synthetic procedure of isotopic enrichment of oxalate in COM phase Et* is used here to designate the ^{13}C-labeled diethyl oxalate precursor enriched on the carbonyl (C$_2$H$_5$O$_2$^{13}C)$_2$), which was used for preparing ^{13}C- and ^{13}C/^{17}O-COM. Bottom: chemical structures of the samples prepared for this study and their abbreviations used in the text. In the saponification reaction, based on the mechanism of this reaction, only one oxygen per function gets isotopically enriched; however, the label is distributed between both oxygen sites, due to the resonance of the carboxylate group, and as evident from ^{17}O ssNMR analysis.
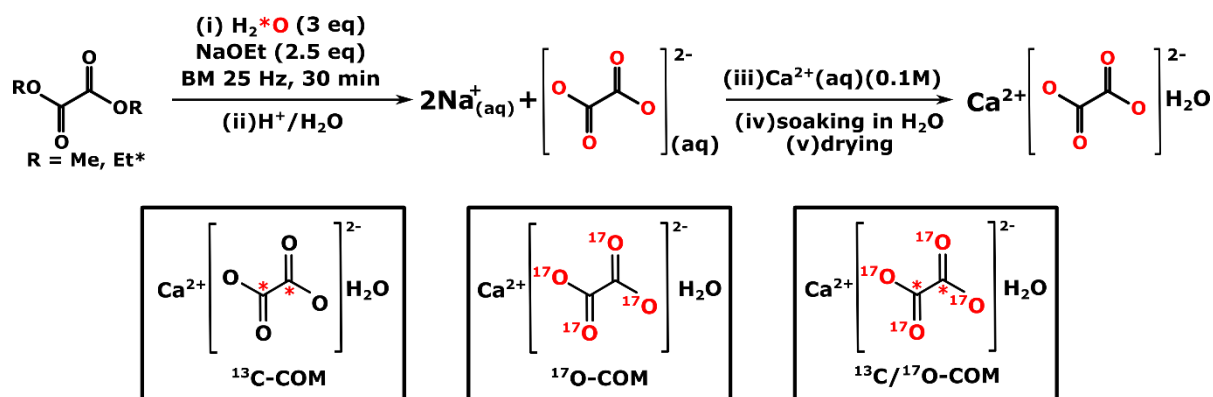
Preparation of anhydrous calcium oxalate mineral ([17]O-COA)

Anhydrous calcium oxalate for ^{17}O NMR studies was obtained by *in situ* dehydration of ^{17}O-COM in the NMR instrument. The COM sample was packed in a 4 mm rotor (with the rotor sleeve and cap made of zirconia); the initial mass was 98.2 mg. The rotor was then introduced in a Bruker 4 mm WVT probe equipped with a Bruker booster BVTB 3500. Heating was performed using hot gas by progressively increasing the temperature up to 220 ^{0}C, while spinning at a frequency of 12 kHz. Nitrogen gas was used for the sample spinning to ensure no rehydration occurred during the cooling process back to room temperature. After the experiment, the rotor was removed from the magnet and immediately moved to the glove box (Argon atmosphere), where it was transferred and repacked to a 2.5 mm rotor in view of further ssNMR experiments at 17.6 T.

Characterization techniques

Infrared (IR) spectra were recorded on a Perkin Elmer Spectrum 2 FT-IR instrument (optical resolution of 0.5 cm^{-1}) in attenuated total reflectance (ATR) measurement mode. Analyses were performed in the 400 – 4000 cm^{-1} range by averaging 4 acquisitions per sample.

Powder XRD (pXRD) analyses were performed on an X'Pert Pro diffractometer using CuKα1-2 radiation (λ = 1.5406/1.5444 Å) with the operating voltage and current maintained at 40 kV and 25 mA, respectively. Diffractograms were recorded between 5° and 60° in 2θ, with a step size of 0.017° in approximately 8 minutes.

In situ pXRD analyses were performed under air on a Malvern-Panalytical Empyrean diffractometer with an Anton-Paar HTK16 high-temperature chamber using CuK$_{α1-2}$ radiation (λ = 1.5406/1.5444 Å). The data were collected between 5° and 50° in 2θ, with a step size of 0.013° and a total recording time of 50 minutes. The sample was suspended in ethanol and then deposited on a Pt-Rh (10%) strip. Ethanol was left to evaporate before starting the heat treatment. The heating rate was set to ~10 ^{0}C per minute, and once the desired temperature was reached, the diffraction powder pattern was recorded.

The pXRD analysis of the [17]O-COA sample recovered after *in situ* NMR experiments was recorded on a Bruker D8 A25 machine using CuK$_{\alpha 1-2}$ radiation (λ = 1.5406/1.5444 Å). The data was collected between 17° and 60° in 2θ, with a step size of 0.025° and an effective detector counting time of 192 s

High-Resolution Mass Spectrometry (HRMS) analyses of enriched sodium oxalate samples were performed on a Synapt G2-S (Waters, SN: UEB205) mass spectrometer operating in a negative mode. Capillary and cone voltages were set to 3000 V and 30 V, respectively. Source and desolvation temperatures were 250 and 100 ^{0}C, respectively. Data were processed using the MassLynx V4.2 software.[41] The HRMS analyses enabled an estimation of the enrichment level within the samples. For example, when using ~99% H$_2^{18}$O enriched water, the enrichment level was found to be ~45%, while when using ~40% H$_2^{17}$O, it was ~19% (Figure S6).

Solid-state NMR experiments

ssNMR experiments were performed at multiple magnetic fields (9.4, 14.1, 17.6, 18.8 and 35.2 T) at different NMR facilities (ICGM in Montpellier, CEMHTI facility in Orléans, and NHMFL in Tallahassee). The spectra were acquired under magic angle spinning (MAS) conditions with spinning frequencies varying from 4 to 30 kHz, and in some cases, using temperature regulation, as specified in Table S1. Chemical shifts were referenced as follows: [17]O to tap water at 0.0 ppm (which corresponds to D$_2$O at *ca* -2.7 ppm, D$_2$O being the IUPAC recommended reference);[42] [13]C to adamantane's high-frequency peak at 38.5 ppm (with respect to tetramethylsilane (TMS)).[43]

In some of the experiments listed below, SPINAL-64 ^{1}H decoupling[44,45] was applied during the evolution and/or acquisition period. The RF fields used for decoupling are given in Table S1.

^{17}O solid-state NMR

Part of the ^{17}O NMR experiments were performed at 14.1 T on a Varian VNMRS spectrometer (ICGM), using 3.2 mm HX or HXY probes operating at [17]O and [1]H Larmor frequencies of 81.31 and 599.82 MHz, respectively. At this field, 1D ^{17}O MAS (Bloch decay) NMR spectra were recorded using a 1.0 µs pulse for excitation (corresponding to a 22.5° tilt angle on a liquid).

At 17.6 T (CEMHTI), the ^{17}O MAS NMR spectra were recorded on a Bruker Avance III HD NMR spectrometer equipped with a 2.5 mm probe operating at a [17]O Larmor frequency of 101.70 MHz. The 1D [17]O Hahn echo experiments were performed with one rotor period echo delay (33.33 µs), using π/2 and π pulse lengths of 8 and 16 µs, respectively. 2D MQ (multiple-quantum) MAS experiments were recorded with excitation, conversion and central transition selective pulse lengths of 2.8, 1.1 and 7.5 µs, respectively. To avoid rehydration of the anhydrous calcium oxalate phase (COA), ssNMR analyses

were performed under N_2 gas spinning; only a very weak ^{1}H resonance (corresponding to water) was observed after 3 days of acquisition.

At 18.8 T (NHMFL), ^{17}O MAS NMR experiments were performed on a Bruker Avance III HD 800 MHz NMR spectrometer using a 3.2 mm Low-E triple-resonance MAS probe operating at a ^{17}O Larmor frequency of 108.47 MHz. 1D ^{17}O experiments were recorded using a Bloch decay NMR pulse sequence, with an excitation pulse length of 3 µs. 2D shifted-echo MQ MAS spectra were acquired with excitation, conversion and central transition selective pulse lengths of 3, 1 and 5 µs, respectively. An additional 2D shifted-echo MQ-MAS with ^{17}O{^{1}H} REDOR (Rotational Echo Double Resonance) recoupling experiment[46] was performed using 8 µs π pulses on the ^{1}H channel, with a total recoupling time of 0.5 ms.

At 35.2 T (NHMFL), ^{17}O MAS NMR spectra were acquired on the Series Connected Hybrid (SCH) magnet,[47] using a Bruker Avance NEO NMR spectrometer equipped with a 3.2 mm single-resonance MAS probe operating at a ^{17}O Larmor frequency of 203.36 MHz. The spinning frequency was set to 10 kHz with temperature control at +10 ºC. The 1D ^{17}O Hahn echo experiment was recorded using one rotor period echo delay, and π/2 and π pulse lengths of 5.0 and 10.0 µs, respectively. No ^{1}H decoupling was applied for this experiment. 2D shifted-echo MQMAS experiments were recorded with excitation, conversion and central transition selective pulse lengths of 3.3, 1.6 and 10 µs, respectively. Because of possible instrumental interruptions such as magnet tripping at 35.2T, these MQMAS experiments were recorded as four 2D acquisitions, which were then added together later for better signal-to-noise ratio. The following equations[48] relate the chemical shift in the indirect dimension (δ_1) of MQMAS experiment to the isotropic chemical shift (δ_{iso}):

$$\delta_1 = \delta_{iso} - \frac{10}{17}\delta_{qis} \tag{1}$$

where the value of δ_{qis} for I=5/2 is given by:

$$\delta_{qis} = -6000 \times \frac{C_Q^2}{v_0^2}\left(1 + \frac{\eta_Q^2}{3}\right) \tag{2}$$

In equation (2) C_Q is the quadrupolar coupling constant, v_0 the Larmor frequency, and η_q the asymmetry parameter.

Complementary information on all ^{17}O ssNMR experiments can be found in supporting information (Table S1).

^{13}C NMR and ^{13}C-^{17}O correlation NMR experiments

One-dimensional (1D) ^{13}C ssNMR experiments were recorded on a VNMRS 14.1 T NMR spectrometer (ICGM), using a Varian 3.2 mm HX probe tuned to ^{1}H and ^{13}C (Larmor frequencies of 599.82 and 150.81 MHz, respectively). The spectra were acquired under MAS, using a cross-polarisation (CP) sequence, with a 3.3 µs excitation pulse on the ^{1}H channel, followed by a ramped spin-lock pulse of 1.5 ms.

1D and 2D ^{13}C/^{17}O MAS NMR experiments were recorded at the NFMFL on a Bruker Avance III HD 800 MHz (18.8 T) NMR spectrometer using a 3.2 mm Low-E probe in triple resonance mode, tuned at frequencies of 201.19 (^{13}C), 108.47 (^{17}O) and 800.12 MHz (^{1}H). The 1D CPMAS experiment was recorded using 3 µs pulse for ^{1}H excitation, followed by a ramped contact pulse of 1.5 ms. A two-dimensional (2D) homonuclear ^{13}C refocused INADEQUATE experiment with z-filter[49] was recorded using the same CP conditions as for the 1D ^{13}C NMR experiment, with further ^{13}C $\pi/2$ and π pulse lengths of 4 and 8 µs, respectively.

2D heteronuclear ^{13}C-^{17}O MAS spectra were recorded at different temperatures using a MQ/D-RINEPT pulse sequence,[50] and $SR4_1^2$ dipolar recoupling.[51] The triple quantum (3Q) excitation, conversion, and central transition selective pulse lengths were 4, 1.4 and 5 µs, respectively, followed by a D-RINEPT-based magnetization transfer with $\pi/2$ and π pulse lengths of 4 and 8 µs, respectively. The $SR4_1^2$ based recoupling sequence was applied on the ^{13}C channel.

In situ high-temperature ^{17}O and ^{13}C NMR experiments

The high field *in situ* high-temperature 1D ^{13}C and ^{17}O MAS NMR experiments were recorded at 17.6 T (CEMHTI) on a Bruker Avance III HD spectrometer equipped with a 7.0 mm Bruker laser-heated MAS double resonance probe operating at ^{1}H and ^{13}C (or ^{17}O) Larmor frequencies of 750.13 and 188.13 (or 101.70) MHz, respectively. A bottomless 7.0 mm MAS rotor was used, equipped with an inner aluminium nitride (AlN) container. Heating of the sample was achieved using a 200 W DILAS diode laser operating at 980 nm up to 470 ^{0}C.[52] The temperature was calibrated using KBr and following the ^{79}Br chemical shift change as a function of the laser power used.[53] *In situ* high-temperature 1D ^{13}C MAS NMR experiments were recorded at a spinning speed of 4 kHz, using a single pulse acquisition (Bloch decay) with a ^{13}C $\pi/2$ pulse length of 7 µs. At each temperature, ^{1}H NMR experiments were performed to monitor the water signal and follow its decrease in intensity (spectra available on demand). At 220 ^{0}C, the sample was left spinning until no more ^{1}H water signal was observed to ensure complete dehydration of the COM mineral, yielding an anhydrous phase.

Complementary *in situ* high-temperature experiments were recorded at 9.4 T (CEMHTI) on a Bruker Avance I NMR spectrometer equipped with a 4.0 mm WVT probe operating at ^{17}O Larmor frequency of 54.18 MHz, and spinning at 12 kHz. 1D ^{17}O DFS Hahn echo experiments were performed using a 1 ms DFS-pulse with a sweep between 200 kHz and 1 MHz, prior to the $\pi/2$ and π pulses of the echo (8

and 16 μs), separated by an echo delay of one rotor period (83.3 μs). Additional T_1 measurements were performed under 12 kHz MAS using a saturation recovery experiment at RT and 200 °C. The saturation recovery experiments were performed using ~100 presaturation pulses (each 10 μs long separated by 1 ms), followed by 5.5 and 11 μs π/2 and π pulses, respectively. Following these analyses, the formed anhydrous COA sample was unpacked in the glove box and analyzed by pXRD, as mentioned above.

Nitrogen gas was used for spinning the rotors on both spectrometers to ensure no rehydration occurred during the experiment and the cooling process.

Computational studies

The optimization of atomic positions for LT-COM was carried out starting from the crystallographic data reported by Daudon *et al*.,[54] as described elsewhere.[36] In brief, the geometry of the structure was optimized progressively: first, proton positions, then oxygen atoms directly bonded to hydrogen atoms, and finally, all atoms.

A model of the relaxed HT-COM structure (supercell size of 2×2×2) was kindly provided by Margarita Shepelenko and co-workers (Weizmann Institute of Science) to deal with the partial occupancies of the experimental structure (see Figure S7 in SI for a representation of the supercell).

The crystal structure of the anhydrous calcium oxalate (α-polymorph) was taken from the work by Izatulina *et al*. (CCDC 1846250).[17] Atomic positions were relaxed using the Vienna *Ab initio* Simulation Package (VASP),[55,56] based on the Kohn-Sham DFT, and using a plane-wave pseudopotential approach with an energy cut-off of 400 eV, and a $2 \times 3 \times 4$ *k*-point mesh for the anhydrous phase. During the geometry optimization, unit cell parameters were kept fixed.

NMR parameters were calculated for all structures using the QUANTUM-ESPRESSO code,[57] keeping the atomic positions equal to the values previously determined using VASP. The Perdew-Burke-Ernzerhof (PBE) generalized gradient approximation was used,[58] and the valence electrons were described by norm-conserving pseudopotentials[59] in the Kleinman-Bylander form.[60] The shielding tensor was computed using the GIPAW approach.[61] The wave functions were expanded on a plane wave basis set with a kinetic energy cut-off of 80 Ry. The calculations were done using a *k*-space mesh density of ~0.04 Å^{-1}.

The isotropic chemical shift δ_{iso} is defined as $\delta_{iso} \approx -(\sigma_{iso}-\sigma_{ref})$, where σ_{iso} is the isotropic shielding and σ_{ref} is the isotropic shielding for the same nucleus in a reference system.[62] Different structures were selected to establish a relevant reference chemical shift for ^{17}O (Table S2). In this work, the value used for σ_{ref} was 228 ppm (slope kept at -1; Figure S8). This σ_{ref} value was derived from comparisons between the calculated shieldings (σ_{iso}) with experimental isotropic shifts (δ_{iso}), for a selection of compounds involving Ca$^{\cdots}$O and/or C-O bonds, as present in the Ca-oxalate structures studied here. The list of

reference structures (amino acids, oxalic acid, calcite and wollastonite) and their ^{17}O NMR parameters are reported in Tables S2 and S3. It is important to highlight that the inclusion of several oxygen environments involving Ca···O bonds was found to be essential to account for the partial Ca-3d O-2p hybridization[63], and thereby establishing a "reasonable" value of σ_{ref} to be used for NMR calculations on Ca-oxalates (as here our Ca pseudopotential used was not corrected for this effect). Indeed, when using previously reported σ_{ref} values (*e.g., ~* 260 ppm), calculated ^{17}O chemical shifts for oxalate oxygen atoms were systematically off by more than 30 ppm.[36,64]

The quadrupolar moments (Q) used to calculate the ^{17}O quadrupolar coupling constant C_Q was -2.558 fm^2.[65] Regarding the chemical shift anisotropy (CSA) parameters, we used here Herzfeld-Berger convention.[66] Further terminology and definitions for chemical shift and quadrupolar parameters are given in the SI and previous work.[36]

MD (Molecular Dynamics) simulations were carried out with the CP2K code[67] consisting in Born–Oppenheimer MD (BOMD) with PBE electronic representation, including the Grimme (D3) correction for dispersion,[68] GTH pseudopotentials,[69] combined plane-wave, and TZVP basis sets.[70] The BOMD was performed using the NVT ensemble, and Nose–Hoover thermostat was used to control the average temperature at 300 or 320 K. Trajectories were accumulated over ~4 ps with a time step of 0.5 fs, and ^{17}O NMR calculations were performed with QE, with averaging done every 100 or 200 steps, *i.e.,* every 50 fs or 100 fs, for 300 and 320 K, respectively.

All calculated structures as well as further computational details are available upon reasonable demand.

All spectra which had been recorded on a Varian VNMRS console were converted to the TOPSPIN software (https://www.bruker.com/en.html), and further processed there. Depending on the experiment, an exponential line broadening was applied to the spectra prior to the Fourier transform. To extract quadrupolar and chemical shift parameters, ^{17}O MAS NMR spectra were fitted using the ssNAKE software.[71] 2D ^{17}O MQMAS spectra recorded at 35.2T were summed for a better signal-to-noise ratio using a MATLAB[72] script written by I. Hung.

Results & Discussion

High-resolution ^{17}O ssNMR of LT-^{17}O-COM: monitoring the diversity of oxalate binding environments

To explore calcium oxalate phase transitions *via* oxygen-17 ssNMR, an isotopically-enriched version of LT-COM was synthesized, using ^{17}O-labeled oxalate ligands prepared by mechanochemistry (Scheme 1). For the first experiments, ~40% ^{17}O-enriched water was used in the labeling step, leading to an average enrichment level ~19% per oxygen, according to HRMS (Figure S6). The ^{17}O MAS ssNMR spectrum of LT-^{17}O-COM is presented in Figure 2a. The high enrichment level of the oxalate oxygen atoms within this sample resulted in excellent sensitivity, allowing the spectrum to be recorded in less than 6 minutes at 18.8 T. The ^{17}O resonances were detected in the spectral region characteristic of carboxylate groups, [28–32] but with no direct resolution over the eight inequivalent oxalate oxygen sites expected from the LT-COM crystal structure, due to the quadrupolar broadening.

To achieve higher resolution, a 2D MQ MAS experiment was performed (Figure 2b). All oxalate sites could thus be resolved, as shown by looking at the spectra of the different "slices" and their individual fits (see Figure S9). ^{17}O MAS NMR spectra of LT-COM were then recorded at different magnetic fields (9.4, 14.1 and 18.8 T) and fitted (Figure S10). The extracted average chemical shift (δ_{iso}) values and quadrupolar parameters (C_Q and η_Q) for each site are reported in Table 1. The chemical shift range was found to span over only 11 ppm for these eight inequivalent sites (between 254 and 265 ppm). C_Q and η_Q values were also very similar, ranging from 7.1 to 7.5 MHz in the former case, and from 0.40 to 0.53 in the latter. A complementary MQMAS analysis was carried out at ultra-high magnetic field (35.2 T) to extract the CSA parameters δ_{cs} and η_{cs} of individual sites (Figure S11 and Table S4). Despite the uncertainties related to some peaks overlapping at this magnetic field, similar values were again found for all sites, with estimated δ_{cs} between -163 and -200 ppm, and η_{cs} between 0.6 and 0.9.

As previous ssNMR analyses of COM had shown the usefulness of *ab initio* calculations to help rationalize the experimental NMR spectra,[36,73,74] DFT-GIPAW calculations were carried out, focusing on the ^{17}O NMR parameters of oxalate oxygen atoms (Table S5). No straightforward one-to-one correlation between experimental and calculated parameters for the different sites could be established. The absolute values of the calculated quadrupolar coupling constants were systematically higher than the experimental ones, reaching ~ 8.2 MHz for several sites (up to ~ 1 MHz more than some experimental values). Similarly, the calculated δ_{iso} values were found to span over ~14 ppm, instead of 11 ppm experimentally. The calculated absolute values of δ_{CS} were also found to be, on average, ~80 ppm higher compared to the experimentally determined ones (Tables S4 and S5). Such discrepancies between the calculated and experimental parameters can be explained by the lack of inclusion of dynamics within these calculations: DFT calculations are carried out at 0 K considering no molecular motions of atoms, while the experimental data was recorded close to room temperature. As shown for

other systems, local atomic/molecular motions within the lattice (notably of the nearby water molecules) can lead to the averaging of the electronic environments of oxalate oxygen atoms and partial averaging of NMR parameters.[30,36,75,76] Preliminary molecular dynamics (MD) simulations were thus carried out at 300 K, followed by GIPAW-DFT calculations of structures extracted along the MD steps, to see how motions within the LT-COM lattice affect the ^{17}O parameters of the oxalate oxygen atoms. As shown in Figure S12, the resulting calculated δ_{iso} and C_Q values at 300 K were found to differ from those at 0 K, the extent of variation depending upon the oxygen site considered. Yet, the relative order of these calculated δ_{iso} values was still inconsistent with our LT-COM experimental assignments. Hence, the influence of smaller changes in temperature was investigated by performing a similar MD simulation at 320 K. This led to further changes in some of the relative orders of δ_{iso} and C_Q of the different sites. Overall, such calculations clearly point to a strong dependence of the oxalate ^{17}O NMR parameters on temperature, as described later in the manuscript, and further underscores the importance of being able to perform *experimental* assignments of the oxalate resonances.
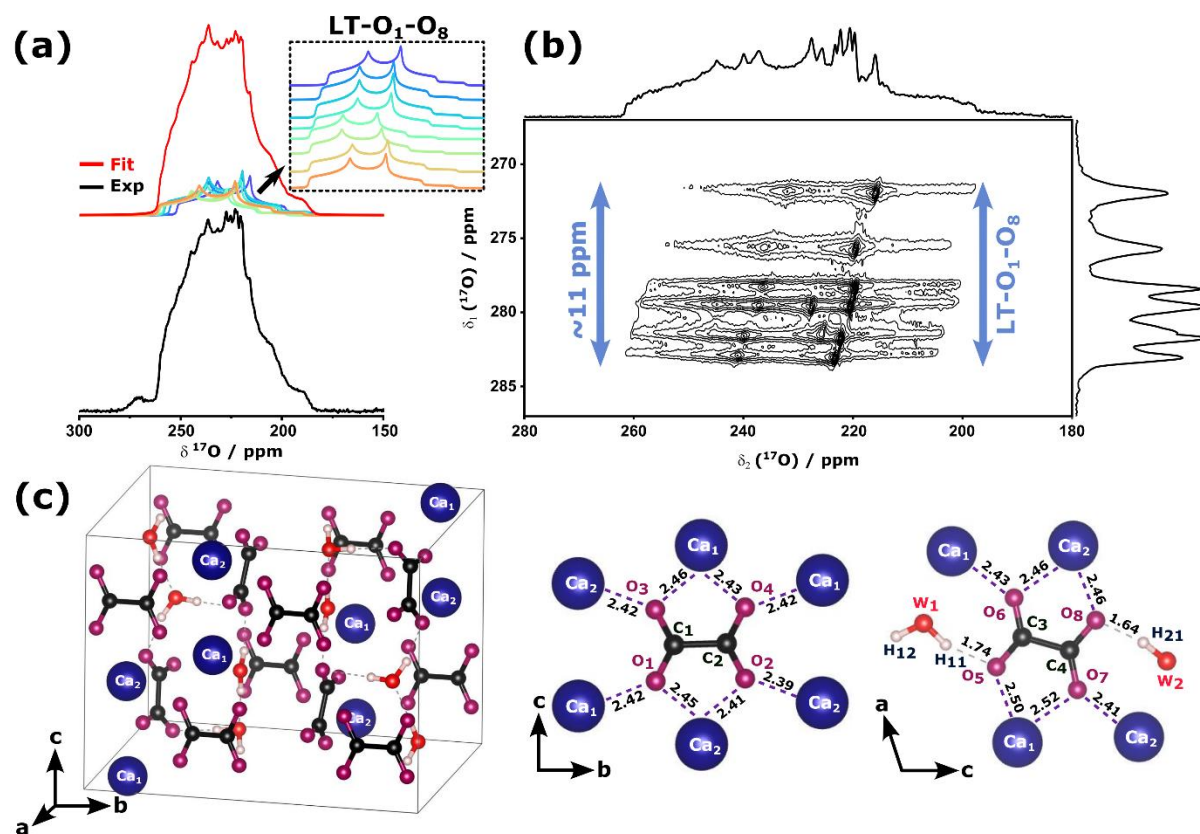

Figure 2. (a) 1D ^{17}O MAS NMR spectrum of LT-^{17}O-COM (in black), and its fit considering eight oxalate oxygen sites (in red); the inset shows the contribution from individual sites. (b) 2D ^{17}O MQMAS NMR spectrum of the same sample showing 8 oxygen sites within a ~ 11 ppm range (LT-O_1 – O_8). Extracted slices and their fits can be found in the SI (Figure S10), and the NMR parameters of each site are reported in Table 1. Both spectra were recorded at 18.8 T, using a MAS frequency of 16 kHz; further experimental details are in Table S1. (c) Representations of the structure of LT-COM along different

crystallographic orientations (with the same color code for atoms as in Figure 1); distances reported are those of the crystal structure (CCDC 1428017).[54]

Table 1. Average experimental ^{17}O NMR parameters for all oxygen sites of LT, HT-^{17}O-COM and ^{17}O-COA samples studied in this work. See Figures S9, S10, S14, S15, S19 and S20 for the experimental spectra and multifield fits, and Table S1 for experimental acquisition parameters.

Compound (Figure)	δ_{iso} (ppm)	$|C_Q|$ (MHz)	η_Q	Assignment	Magnetic Field (T)
LT-^{17}O-COM (Figure 2)	254.1 ± 0.1	7.27 ± 0.02	0.52 ± 0.01	LT-O_7	9.4, 14.1 and 18.8
	258.3 ± 0.3	7.30 ± 0.02	0.50 ± 0.01	LT-O_6	
	259.9 ± 0.2	7.41 ± 0.04	0.53 ± 0.01	LT-O_1/O_3	
	260.8 ± 0.1	7.45 ± 0.01	0.53 ± 0.01	LT-O_2/O_4	
	262.9 ± 0.2	7.49 ± 0.02	0.51 ± 0.01	LT-O_1/O_3	
	263.9 ± 0.1	7.50 ± 0.01	0.50 ± 0.01	LT-O_2/O_4	
	264.0 ± 0.4	7.07 ± 0.03	0.45 ± 0.01	LT-O_8	
	264.8 ± 0.6	7.31 ± 0.04	0.40 ± 0.01	LT-O_5	
HT-^{17}O-COM (Figure 5)	256.0 ± 0.5	7.13 ± 0.02	0.55 ± 0.01	HT-O_{11}	9.4, 14.1, 17.6 and 18.8
	262.8 ± 0.4	7.49 ± 0.01	0.52 ± 0.01	HT-O_9	
	264.4 ± 0.5	7.12 ± 0.01	0.50 ± 0.01	HT-O_{10}	
^{17}O-COA (Figure 6)	242.6 ± 0.1	6.96 ± 0.10	0.74 ± 0.01	A-O_{15}	17.6 and 9.4
	256.3 ± 0.1	7.47 ± 0.05	0.49 ± 0.01	A-O_{12}/O_{13}	
	261.7 ± 0.1	7.47 ± 0.01	0.52 ± 0.01	A-O_{12}/O_{13}	
	282.4 ± 0.1	7.88 ± 0.08	0.24 ± 0.01	A-O_{14}	

To help gain resolution, a doubly labeled sample (enriched in ^{13}C and ^{17}O) was prepared. The LT-$^{13}C/^{17}O$-COM phase was synthesized starting from 99% ^{13}C-labeled diethyloxalate (enriched on both carboxyl carbon atoms) and using ~90% $H_2^{17}O$ for the mechanochemical saponification step, leading to an average ^{17}O-enrichment level ~40-45% on the oxalate oxygen atoms (as estimated from our previous experience on such labeling reactions).[38,40] First, the 1D ^{13}C NMR spectrum was recorded (Figure 3a, top). Due to the very high ^{13}C-enrichment level in LT-$^{13}C/^{17}O$-COM, the spectrum is significantly broadened compared to the non-enriched COM phase (Figure 3a, bottom) due to the J coupling and n ~0 rotational resonance of the dipolar coupling between two ^{13}C with close isotropic shifts, but different CSA tensor orientations. While four resonances are resolved in the one-dimensional ^{13}C CPMAS NMR spectrum of non-labeled LT-COM at 20 ^0C (with the inequivalent carbon sites

assigned as proposed by Colas *et al.*),[73] high-resolution in ^{13}C could only be achieved in the case of the doubly labeled LT-^{13}C/^{17}O-COM phase by using a two-dimensional homonuclear ^{13}C-^{13}C INADEQUATE experiment (Figure 3b). Indeed, the two sets of signals corresponding to the two inequivalent oxalate ions are thus resolved (Figure 3b), where the higher frequency signals correspond to C_3 and C_4, and the lower ones to C_1 and C_2 (Table 2 and Figure 3c). Subsequently, the doubly labeled phase was studied using a 2D heteronuclear ^{13}C-^{17}O MQ/D-RINEPT experiment. The $SR4_1^2$ dipolar recoupling scheme was used, with a short recoupling time, so that the cross-peaks correspond to the directly bound ^{13}C-^{17}O atoms.[51] The four oxygen atoms belonging to each inequivalent oxalate ion were thus separated, as shown in Figure 3d, where the beige and blue-shaded zones correspond to the signals arising from the two different oxalate ions. This enabled to determine, for each of the 4 inequivalent oxalate carbon atoms, which two oxygen resonances correspond to the atoms directly linked to them (Table 2). Further discrimination between the two oxygen atoms bound to the same carbon (*e.g.,* O_5 *vs* O_6, or O_7 *vs* O_8), was achieved by probing the $^{17}O^{\cdots 1}H$ proximities in LT-^{17}O-COM using 2D MQMAS in combination with $^{17}O\{^1H\}$-REDOR. According to the crystal structure (Figure 3c), O_5 and O_8 are involved in hydrogen bonding, while O_6 and O_7 are not (nor O_1 to O_4), meaning that the former oxygen sites should be distinguishable on the basis of their higher $^{17}O^{\cdots 1}H$ dipolar couplings, *i.e.*, proximities. Figure 3e shows a comparison of the ^{17}O δ_1 dimension of the $^{17}O\{^1H\}$ MQ/REDOR experiment, performed without (black) and with (red) ^1H recoupling of 0.5 ms. No change in the signal intensities were observed for the two lower frequency resonances (centered at 271.8 and 275.1 ppm), while a small amount of dephasing is noticeable for signals in the range between 277 - 285 ppm, implying that O_5 and O_8 are in the higher shift zone (Table 2). (Here, it is the $\delta_1(^{17}O)$ values that are considered, which differ from $\delta_{iso}(^{17}O$, as detailed in the experimental section). Although a more complete assignment of each of the oxygen resonances of the other oxalate ligand (blue-shaded zone) could not be performed at this stage, it should nevertheless be highlighted that this is the first time that ^{17}O NMR spectra showing the oxalate resonances of LT-COM are reported, with the eight oxygen sites being fully resolved using ^{17}O MQMAS and ^{13}C-^{17}O MQ/D-RINEPT experiments. This is all the more noteworthy considering the similar oxygen local environments and the small isotropic chemical shift range of only ~ 11 ppm. Thus, this demonstrates the potential of high-resolution ^{17}O NMR for finely investigating the structure of oxalate-based materials. Based on these first results, we then decided to look into the successive phase transitions of LT-COM upon heating, focusing on the signatures of the oxalate oxygen atoms.
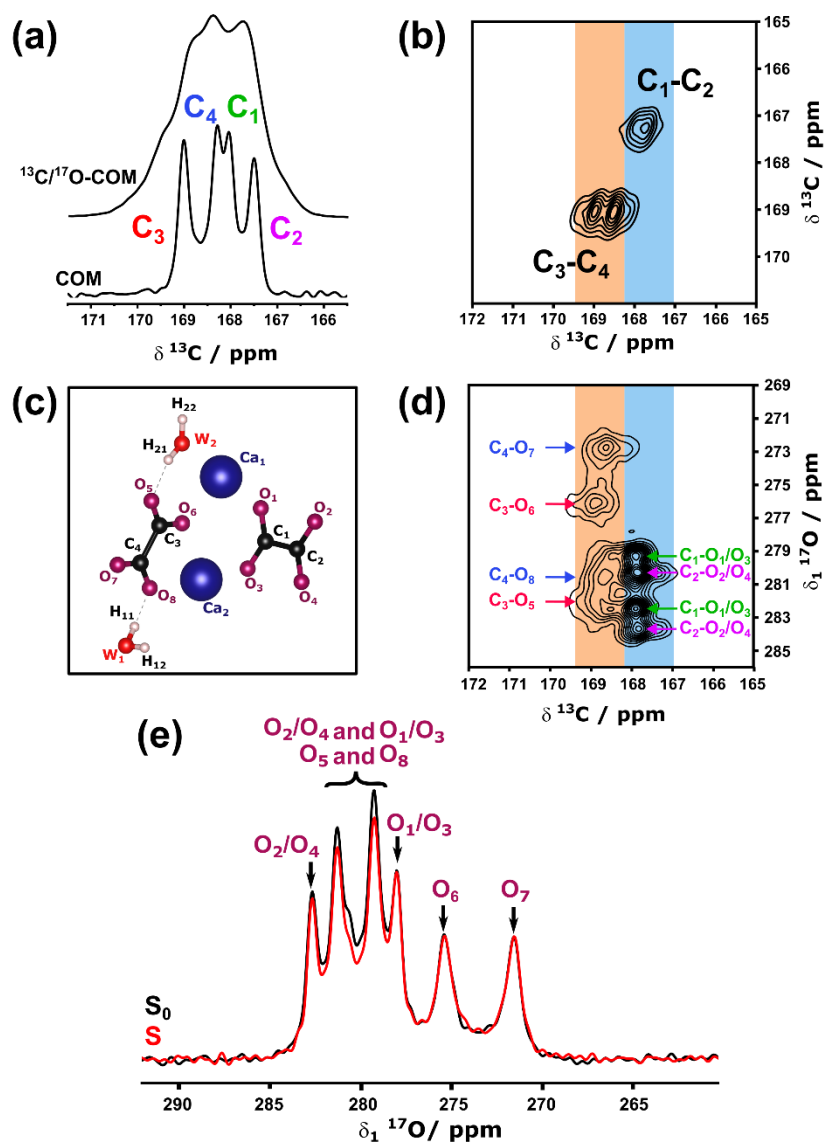
Figure 3. (a) [13]C 1D CPMAS spectra of LT-COM at natural abundance (bottom) and for the doubly enriched ^{13}C/[17]O phase (top). (b) Homonuclear 2D [13]C-^{13}C INADEQUATE at +20 [0]C with the assignment of the carbon signals (as proposed according to Colas *et al.*[73]). (c) Crystal structure of LT-COM as reported by Daudon *et al.*[54] (d) 2D heteronuclear [13]C-[17]O MQ/D-RINEPT spectrum of ^{13}C/[17]O-LT-COM recorded at +20 [0]C with a tentative assignment of the cross-peaks. The chemical shifts and assignments derived from spectra (b) and (d) are reported in Table 2. The differences in relative intensities of the cross-peaks probably reflect differences in J couplings. (e) Indirect dimension (δ_1) of the MQMAS [17]O{[1]H} MQ/REDOR experiment carried out on LT-[17]O-COM, recorded with (in red) and without (in black) [1]H-recoupling. The dephasing time used here was 0.5 ms.

Table 2. Chemical shifts and proposed assignment of δ ^{13}C and δ$_1$ ^{17}O resonances, as shown in Figures 2 and 3. δ$_1$ (^{17}O) is a chemical shift in the indirect dimension of the 2D MQMAS experiment, which differs from δ$_{iso}$ (^{17}O) (see experimental section for details how δ$_1$ is calculated and related to the δ$_{iso}$).

2D ^{13}C-^{13}C INADEQUATE		^{13}C-^{17}O MQ/D-RINEPT $SR4_1^2$ & ^{17}O{^{1}H} MQ/REDOR	
δ$_{iso}$ /ppm (δ^{13}C)	Assignment	δ$_1$ /ppm (δ$_1$^{17}O)	Assignment
168.9	C3	275.1	O$_6$
		281.5	O$_5$
168.7	C4	271.8	O$_7$
		279.6	O$_8$
167.9	C1	278.3	O$_1$/O$_3$
		281.5	
167.7	C2	279.3	O$_2$/O$_4$
		282.7	

Phase transition from LT- to HT-COM: following progressive changes in oxalate local environments

As mentioned in the introduction (Figure 1), upon heat treatment up to ~75°C, LT-COM progressively transforms into HT-COM. The latter phase has a different lattice symmetry and presents a positional disorder on the water molecules and some of the oxalate oxygen atoms, based on XRD analyses and computational studies.[17,77] Moreover, recently, we showed using ^{17}O and ^{2}H ssNMR that the water molecules progressively undergo more pronounced molecular motions when transitioning to the HT form.[36] Regarding the oxalate local environments, ^{13}C CPMAS NMR analyses at natural abundance have shown that the 4 resolved inequivalent carbon sites of LT-COM merge into two main resonances upon heat treatment,[26] which is in line with the formation of an HT-COM phase with *I2/m* (equivalent to *C2/m*) symmetry.[77] Here, to follow the transition from the LT- to the HT-COM form more precisely, we performed for the first time variable temperature ^{17}O-^{13}C ssNMR analyses, by looking directly at the local environments of the oxalate oxygens (Figure 4).

The 2D ^{13}C-^{17}O MQ/D-RINEPT NMR spectra of the doubly-labeled ^{13}C/^{17}O-COM sample were recorded at four different temperatures between -30 and +75°C, as shown in Figure 4. From the ^{13}C perspective, the merging of the ^{13}C resonances of each oxalate group (*i.e.,* C$_1$ and C$_2$ on one hand, and C$_3$ and C$_4$ on the other) is observed above +50 °C, leading to the two resolved ^{13}C resonances (noted here C$_5$ and C$_6$ – but which correspond to C$_5$ and C$_1$, respectively, in the initially reported crystal structure by Shepelenko *et al*), as expected from previously reported 1D ^{13}C CPMAS NMR analyses[26] of HT-COM (see the evolution of the ^{13}C as a function of the temperature in Figure S13). From the ^{17}O perspective, it is also possible to follow the oxygen chemical shift changes with respect to the different temperatures. Indeed, a partial merging of the ^{17}O resonances of O$_5$ with O$_8$ (leading to O$_{10}$ in HT-COM), of O$_6$ with O$_7$ (leading to O$_{11}$ in HT-COM) and of the O$_1$-O$_4$ signals (O$_9$ in HT-COM) is observed. Notably, the O$_6$ position moves significantly to lower δ$_{iso}$(^{17}O) chemical shift values with

temperature (comparing -30 and + 50°C data), which is consistent with the evolution of the calculated chemical shift value of this specific site comparing static 0 K (Table S5) and MD averaged results (Figure S12). Such analyses demonstrate the importance of ^{17}O ssNMR. The changes in ^{17}O NMR shifts are more pronounced upon heat treatment than the ^{13}C ones, making it a very sensitive probe to local binding environments. Moreover, while two ^{13}C resonances are resolved for the inequivalent oxalates of HT-COM (C_5 and C_6), three ^{17}O resonances can be distinguished for their oxygens (*i.e.,* two for oxygen atoms coordinated to Ca^{2+} only (O_9 and O_{11}), and one coordinated to Ca^{2+} and involved in H-bonds with water molecules (O_{10})). Hence, ^{17}O ssNMR stands out as a key asset for analyzing crystalline phases involving oxalate ligands in detail by "NMR crystallography", providing direct insight into different oxygen local vicinities.
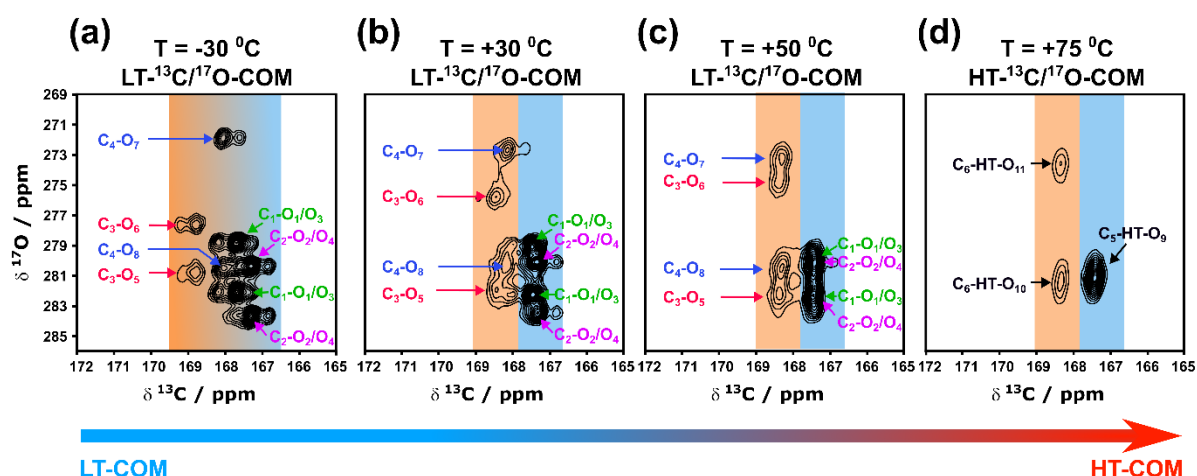

Figure 4. 2D heteronuclear ^{13}C-^{17}O MQ/D-RINEPT spectra recorded at (a) -30, (b) +30, (c) +50 and (d) +75 ^{0}C, showing the evolution of oxygen and carbon sites with increasing temperature. Table S6 shows how chemical shifts are evolving with respect to temperature. The combined contributions of J, dipolar and quadrupolar couplings give rise to the asymmetric appearance of the ^{13}C-^{17}O correlations in the 2D spectra. At higher temperatures, the asymmetry seems to be reduced in intensity due to increased dynamics. The differences in relative intensities of the main cross-peaks probably reflect differences in the ^{13}C-^{17}O J-couplings. Oxygen sites abbreviated in this article as O_9, O_{10} and O_{11} correspond to O_1, O_{13}/O_{14} and O_9, respectively, in the reported crystal structure by Shepelenko *et al.*[20]

Complementary high-resolution ^{17}O NMR analyses of the HT-COM structure were then performed to determine the quadrupolar parameters for the three inequivalent oxygen sites resolved at +75°C (Figure 4d). The 1D ^{17}O MAS and 2D MQMAS NMR spectra are shown in Figures 5, S14 and S15. The fitted NMR parameters extracted from the multiple magnetic field analyses are given in Table 1. Assignments were performed considering both the relative intensity and the ^{17}O chemical shifts of the 3 sites observed

at 75°C (Figure 4d). Overall, the chemical shift range for the HT-COM structure was found to be slightly smaller compared to the LT-COM one, spanning from 256 to 264 ppm. The quadrupolar parameters were similar, with C_Q between 7.1 and 7.5 MHz, and η_Q between 0.50 and 0.55 (Table 1).
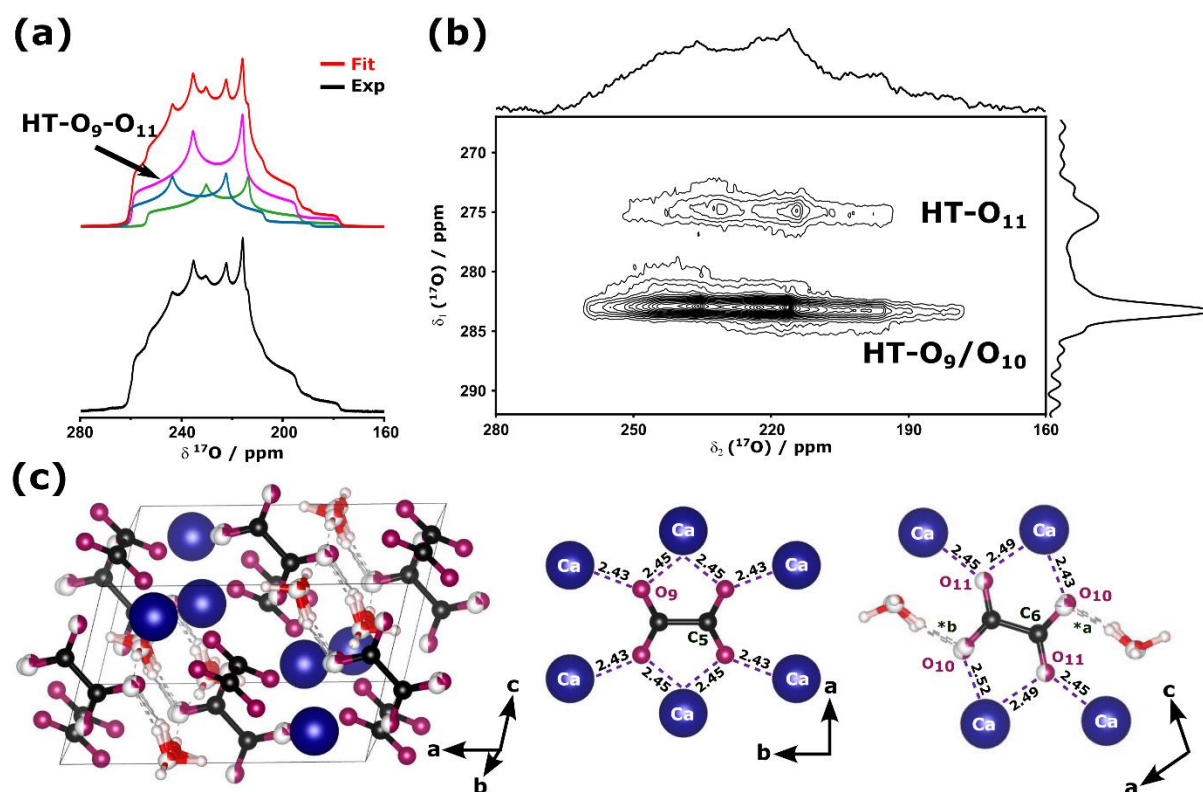

Figure 5. (a) 1D ^{17}O MAS NMR spectrum of HT-COM-^{17}O (in black), together with its fit considering three oxalate oxygen sites (in red); the individual contributions from sites O_9, O_{10} and O_{11} (in pink, blue and green, respectively). (b) 2D ^{17}O MQMAS NMR spectrum of the same sample showing three oxygen sites. Extracted slices with corresponding fits can be found in the SI (Figure S14), while the NMR parameters of each site are in Table 1. Both spectra were recorded at 17.6 T, using a MAS frequency of 30.3 kHz at +80 °C. For further experimental details, see in the Table S1. (c) Representation of the crystal structure of HT-COM, showing the different average orientations of the water molecules in the lattice. Distances reported come from the published crystal structure of Shepelenko et al.[20]. Distances noted *a and *b vary from 1.63 to 2.24 Å, and from 1.63 to 2.39 Å, respectively.

These high-resolution ^{17}O NMR analyses of oxalates in HT-COM provide information about its structure, which is complementary to what was reported in our previous work.[36] First, while the ^{17}O ssNMR spectra of the water molecules in HT-COM had shown a loss in quadrupolar line-shape (which

could be explained by the increased dynamics of these molecules at high temperature), the oxalate ^{17}O NMR parameters and line-shapes of the HT form remain close to those of the LT one. Hence, within the timescale probed by these NMR experiments, it appears that *molecular* motions within the HT-COM structure are essentially centered around the water molecules. The progressive merging of the oxalate ^{13}C and ^{17}O signals with temperature (Figure 4) then attests only to increased local *atomic* motions within the HT-lattice, which results in some of the environments of oxalate oxygens becoming equivalent upon heating (due to resulting distance and angle averaging around them), and in a change in crystal symmetry upon heat treatment. Interestingly, it can be noted that the ^{17}O quadrupolar coupling constants of O_{10} and O_{11} are ~0.3 MHz smaller than for O_9, which may reflect the fact that the former oxygen sites are in closer proximity to the water molecules and, hence, more sensitive to their movements, leading to a more "averaged" ^{17}O electronic environment for the nearby oxalate oxygen atoms.

In order to go further in the study of the structure and dynamics within HT-COM, and account for all ssNMR observations, a more complete computational study would be required, involving both MD simulations and *ab initio* calculations of NMR parameters using the GIPAW method.[78] Yet, calculations on the HT form are more computationally demanding than on the LT form, due to the change in symmetry at high temperature, implying the need to work on a supercell for HT-COM (Figure S7b). Although preliminary GIPAW-DFT calculations were performed on this structure at 0K (see Table S7 and Figure S16), comprehensive investigations were not performed at this stage.

Formation and characterization of anhydrous calcium oxalate

Upon further heating, COM undergoes dehydration, leading to the formation of anhydrous calcium oxalate (COA, Figure 1). To date, three anhydrous polymorphs have been reported (noted α, β, and γ), and their structure, formation, and interconversion have been studied both experimentally and computationally.[17,18,33] Using *in-situ* pXRD analyses, it was proposed that the α form appears first in the 120 – 150°C range, followed by β around ~310 – 340 °C, and finally γ at ~410 °C.[17] Yet, the exact temperature of appearance of these polymorphs was found to depend on the heating conditions and the nature of the experimental set-ups used (*e.g.,* sample in a capillary or on a platinum strip).[17,33] Moreover, controversial conclusions about the structure of the transient α polymorph were reported. Indeed, among the four computational models of COA proposed by Zhao *et al.*,[33] α-COA was suggested to match with the model noted "COA-III" (*P2/m*), while more recent experimental studies carried out by Izatulina *et al*. concluded that the structural model noted "COA-IV" (*C2/m*) corresponded best to their data.[17] Both proposed models result in similar calculated diffraction patterns, making them difficult to distinguish on the basis of XRD analyses. Here, taking advantage of the [13]C- and [17]O-enriched COM phases, we decided to perform for the first time *in situ* solid-state NMR analyses to investigate the formation of COA*,* and further investigate the structure of the α form.

Because heating to temperatures above ~ 200°C using ssNMR requires specific equipment (*e.g.* a laser-heated probe), the *in situ* heating of the COM sample was first studied on the ^{13}C-COM phase (as ^{13}C is more accessible by ssNMR), to determine how the phase transitions occur under these heating/spinning conditions. Experiments were performed at 17.6 T using a 7 mm MAS probe equipped with an inner-crucible, and sample spinning was done under nitrogen gas to avoid rehydration of the anhydrous forms during the experiments (for further details, see SI). The ^{13}C-COM sample was heated up to 450°C by steps of 25°C, spending ~ 15 minutes at each temperature (Figure 6a and Figure S17), to enable thermalization of the sample in the rotor. ^{13}C NMR experiments were performed at each step using a simple "direct excitation" (Bloch-decay) experiment. ^{1}H NMR experiments were also performed in the first stages of heating, to follow the progressive dehydration of COM. In doing so, it was observed that a residual ^{1}H resonance was initially present on the spectra at 200 °C, and that the sample had to be kept for an additional ~30 minutes at this temperature to ensure full dehydration. In comparison to previous reports on the *in situ* dehydration of COM (notably by pXRD), it appears that a higher temperature is required here to remove all the crystalline water. This could be because the sample–is exposed to additional centrifugal forces and pressure under MAS rotation, which may render the release of water upon dehydration more complex (especially for the crystallites closest to the rotor wall). At this stage, the effects of the spinning on the phase transitions were not further explored. Upon heating between 200 and 450°C, the two ^{13}C resonances of COA were found to progressively shift to higher frequencies (by ~ 0.6-0.8 ppm), most probably due to the thermal expansion of the lattice (see SI, Figure S17, for further discussion).
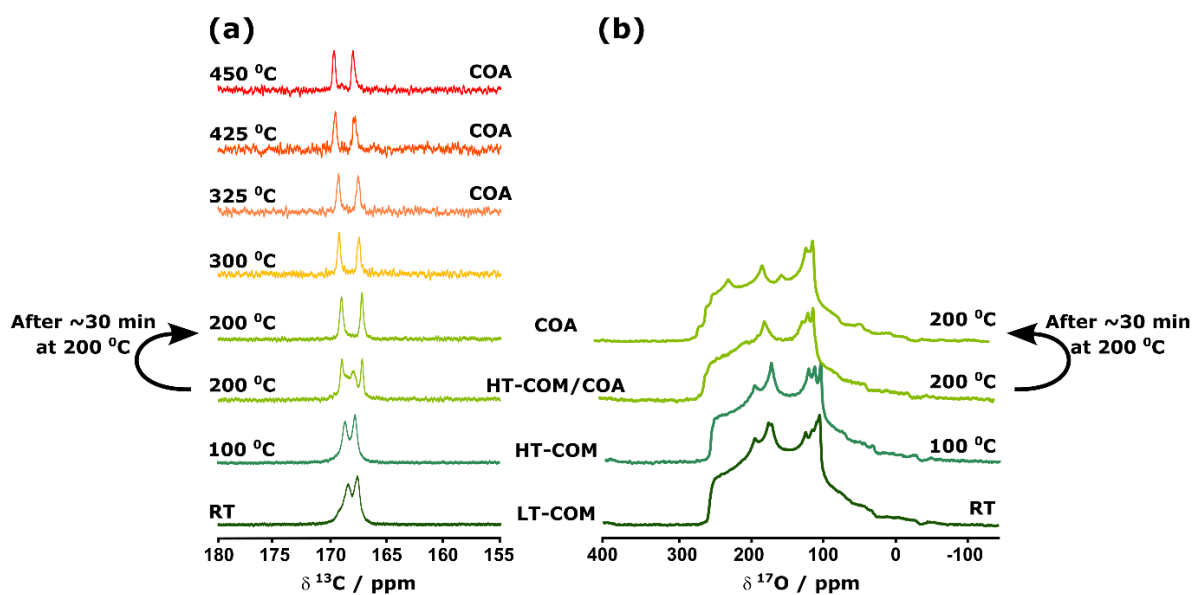
Figure 6. (a) 1D ^{13}C MAS NMR spectra recorded at different temperatures at 17.6 T on the ^{13}C-COM sample (using a 7 mm rotor). (b) 1D ^{17}O MAS NMR experiments recorded at 9.4 T on the ^{17}O-COM sample (using a 4 mm rotor). The ^{17}O NMR spectrum of the COA phase was re-recorded after cooling back to room temperature under N_2 gas flow, showing no change.

Following the high-temperature study of ^{13}C-COM, the heating of ^{17}O-COM was investigated. Yet, in this case, ^{17}O NMR experiments were performed at a lower magnetic field (9.4 T), due to the availability of a better-suited high-temperature probe, adapted to 4 mm diameter rotors. Indeed, this probe turned out to be particularly advantageous for ^{17}O NMR analyses, *(i)* because of the faster spinning speed which can be reached (12 kHz for the 4 mm probe, compared to 5 kHz for the 7 mm one used for ^{13}C NMR), which is important for a quadrupolar nucleus like oxygen-17, and *(ii)* due to the larger amount of sample which can be accommodated in the rotor (~90 mg in the 4 mm rotor, *vs* less than 20 mg in the 7 mm one containing inner-crucibles). The latter point was critical for studying the formation of COA by ^{17}O NMR within reasonable analytical time, due to the significant increase in effective ^{17}O T_1 at higher temperatures (~8 s for COA at 200°C, compared to ~0.1 s for COM at room temperature, see Figure S18), which is likely related to the loss of water.

The 1D ^{17}O NMR spectra of LT-, HT-COM and COA at RT, 100 and 200 °C are presented in Figure 6 (b). At 200 ^{0}C, a significant change in the oxygen-17 line-shape was observed, attesting to COA formation. After cooling the COA sample back to room temperature under N_2 gas (to avoid any rehydration), further analyses were performed at 17.6 T using 1D and 2D MQMAS experiments to resolve the oxygen sites. As shown in Figure 7, four oxygen sites were thus resolved in the ^{17}O-COA phase (Figure S19). The multifield fits of this sample are presented in Figure S20, together with the integrated relative intensities for each site, and their ^{17}O NMR parameters are reported in Table 1.
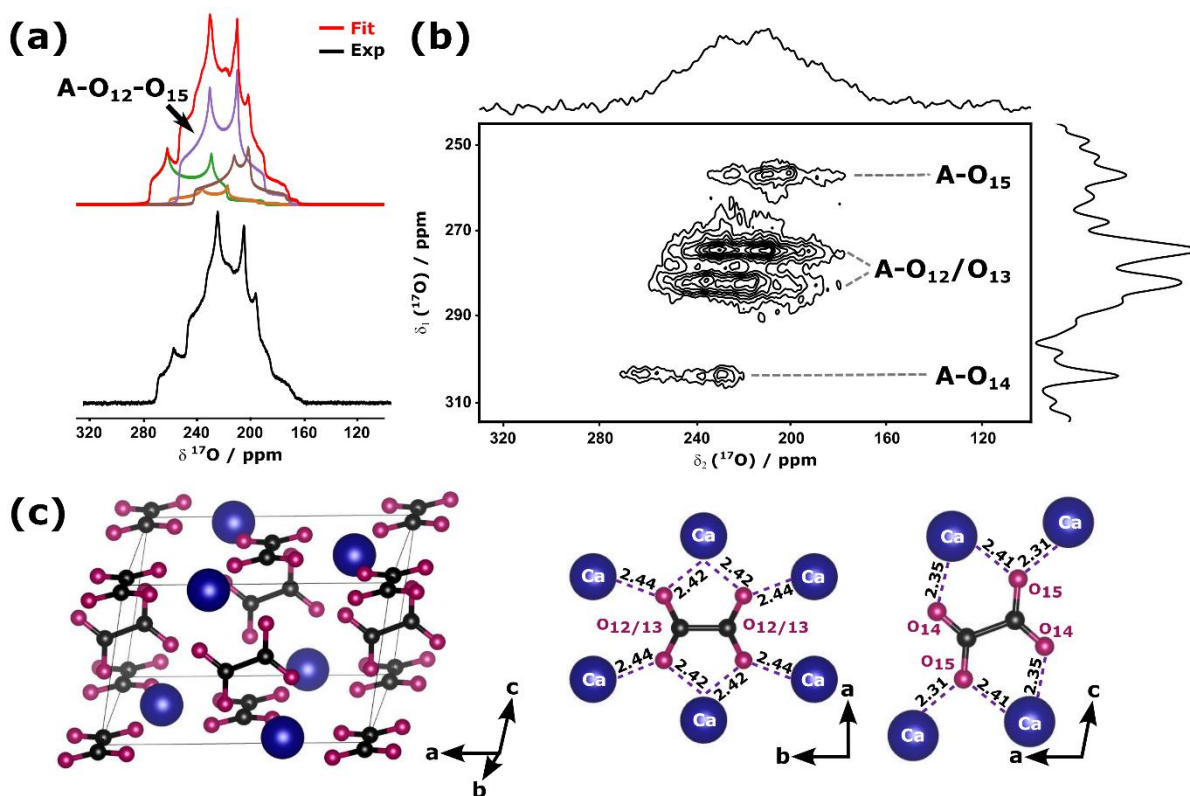
Figure 7. (a) Experimental 1D ^{17}O MAS NMR spectrum of the COA-^{17}O sample (in black), with its overall fit considering four oxalate oxygen sites (in red), the individual oxygen sites being labeled O_{12}/O_{13} (purple and orange), O_{14} (green) and O_{15} (brown). The oxygen sites numbered as O12/O13, O14 and O15 correspond to O2, O3 and O1, respectively, in the reported crystal structure (CCDC 1846250) by Izatulina *et al.*[17] (b) 2D ^{17}O MQMAS NMR spectrum of the same sample showing four oxygen sites (A-O_{12} – O_{15}). Extracted slices and their fits are shown in the SI (Figure S19), and NMR parameters in Table 1. Both spectra were recorded at room temperature at 17.6 T, with a MAS frequency of 30.3 kHz (while spinning under N_2 gas), but a much shorter recycle delay was used for the MQMAS experiment. For further experimental details see Table S1. (c) Representation of the structure of α-COA, which corresponds to the phase which was analyzed by NMR.

Because anhydrous calcium oxalate can exist as different polymorphs, complementary pXRD analyses were performed to help identify the anhydrous ^{17}O-COA phase(s) which had been isolated by progressive dehydration of ^{17}O-COM in the ssNMR probe, and characterized by high-resolution ^{17}O NMR. First, following the ssNMR analyses, the pXRD pattern of the sample was recorded under inert atmosphere: it was found to match the one of the α polymorph (Figure S21). Second, further *in situ* high temperature pXRD analyses were carried out, showing that if the β-polymorph forms at high temperatures (Figure S22), it does not re-transform into the α-phase upon cooling (as also reported in

previous works).[17,33] Thus, it seems clear that the anhydrous phase studied by ^{17}O ssNMR was the α-form.[17]

In the reported crystal structure of α-COA (C2/m space group),[17,33] there are 2 inequivalent carbon and 3 inequivalent oxygen sites, with one of the oxygen atoms placed in a special position. While the high-temperature ^{13}C ssNMR of anhydrous calcium oxalate shows two resonances (Figure 6a), the ^{17}O MQMAS spectrum shows 4 resolved resonances (Figure 7b). The raw crystallographic data of the reported structure was thus re-analyzed in detail. It was noticed that the thermal ellipsoids for two of the oxalate atoms (numbered O_2 and C_2 in the previously reported crystal structure)[17] were more pronounced than the others, suggesting unresolved disorder or the presence of a pseudo-inversion center instead of a real one. To try to reconcile XRD and NMR results, two possibilities were considered: *(i)* a different space group for the crystallographic data (with C2 symmetry, implying notably the symmetry independence of two O2 sites which are symmetry-equivalent in C2/m), and *(ii)* a small disorder around C_2 and O_2 positions within the C2/m space group.

Regarding the first option, attempts to refine the structure in the C2 space group were unsatisfactory: correlations were too large to get a stable refinement and accordingly nice ellipsoids. Moreover, for this possibility to be valid, equal relative intensities of the four oxygen sites should have been observed in the quantitative 1D ^{17}O ssNMR, which is not the case in our fits (see Figure S20). Additionally, we performed a periodic DFT optimization of this structure without imposing C2/m symmetry constraints (*i.e.*, in space group P1), and then analyzed quantitatively the resulting structure with respect to the presence or absence of the symmetry operators of space group C2/m. For this, we used the reciprocal space method developed for the detection of symmetry elements in P1 electron density maps in the context of iterative structure solution methods in crystallography.[79] The results of this symmetry analysis are without any ambiguity: the relaxed P1 structure has true C2/m symmetry. This is in line with the very small (and nearly insignificant) DFT energy drop - 0.49797 eV - obtained after the release of the symmetry constraints in C2/m. Overall, all these analyses tend to show that the C2/m space group is correct, but that the structure presents a small positional disorder on some of the atomic positions.

In ^{17}O ssNMR, the signals attesting of this crystallographic disorder are most likely those which have the most similar NMR parameters (in the central part of the spectrum), with a relative intensity ~ 0.16 (sites referred to as O_{12}/O_{13} in Figures 7, S19 and S20). Assignment of the other two α-COA oxygen sites observed in ^{17}O NMR was performed *(i)* by carefully assessing the structures of the HT-COM and COA, and comparing their relative ^{17}O chemical shifts, and *(ii)* using complementary GIPAW-DFT calculations. First, looking at the relationships between the structures, it appears that O_{10} and O_{11} in HT-COM become O_{14} and O_{15}, respectively, in α-COA (Figure S1). Supposing that the relative isotropic chemical shifts of these two sites remain the same upon formation of the anhydrous form, this would lead to O_{14} being the site with the highest δ_{iso} value (282.4 ppm), and O_{15} the other (242.6 ppm).

GIPAW-DFT calculations were carried out, using as a model for α-COA the previously reported crystal structure (*i.e.,* with no disorder),[33] and relaxing atomic positions (see Table S8). The highest and lowest calculated chemical shifts were found to correspond respectively to O_{14} and O_{15}, and an intermediate shift was found for the remaining oxygen site. The relative order of calculated C_Q and η_Q parameters for these resonances was also found to agree with experimental data, thereby confirming the proposed assignment.

Overall, this study on α-COA further demonstrates the usefulness of ^{17}O ssNMR for analyzing the crystalline structure of oxalate materials in detail. Notably, for this phase, the ^{17}O chemical shift range spans over ≈ 36 ppm, which enabled to resolve a small ^{17}O resonance attesting of positional disorder in the material, with a small occupancy. In contrast, the ^{13}C chemical shift range is much more limited (< 2 ppm), preventing from picking up such subtilies in the structure.

Conclusion

We have successfully shown that oxalate anions can be isotopically enriched in oxygen-17 using mechanochemistry, resulting in a good enrichment level. The given enrichment protocol was used to prepare enriched COM biominerals, where the protocol was further expanded to obtain carbon-13 enriched and even doubly labelled minerals. The prepared samples were then further used to follow by *in situ* ssNMR analyses the phase transitions upon heat-treatment, from the LT to the HT forms of COM, and then the anhydrous α-COA phase. Using high-resolution oxygen-17 ssNMR, it was possible to resolve and assign the ^{17}O resonances, and gain new insight into the structures of these minerals. Notably, ^{17}O NMR was clearly shown to be a very sensitive probe of oxalate binding modes, allowing us to shed light on features that had not been seen so far, including a small amount of positional disorder in α-COA. Given the large number of functional (bio)materials involving oxalate ions, this work expands beyond some of the early ^{17}O solution NMR studies on oxalate binding in biomolecules,[80-81] and clearly demonstrates the added value of using ^{17}O labeling in structural analyses using NMR-crystallography approaches.

Author contributions

The project was conducted by IG, in close interaction with DL. IG carried out the isotopic enrichment experiments, characterizations by IR, MS and pXRD, as well as the vast majority of ssNMR experiments. IH and ZG performed the high-resolution experiments at 18.8 T and 35.2 T (including variable-temperature studies on the LT to HT phase transition), and IH participated to data analysis. VSK participated to the high-temperature ^{17}O NMR experiments recorded at 17.6 T (Orléans) and the study on COA. IG and CG carried out GIPAW DFT computations, CG performed the MD calculations, and DB and DL participated to discussions on computational results. JNS and TXM participated in discussions on mechanochemistry labeling reactions. CG, CL and CB participated in discussions on ssNMR data of calcium oxalates. AVdL performed the crystallographic study of the COA phase. IG and DL wrote the initial draft of the manuscript (deposited as a preprint),[82] and all authors contributed to the final preparation of the article.

Supporting information: Complementary IR, pXRD and MS analyses of the materials; ssNMR acquisition parameters; computational details; fits of ^{17}O NMR spectra of LT- and HT-COM, and of α-COA; variable-temperature ^{13}C NMR spectra, variable temperature pXRD data; representations of the structural correspondence between the different phases. (PDF)

References

(1)   Yeoh, J. S.; Armer, C. F.; Lowe, A. Transition Metal Oxalates as Energy Storage Materials. A Review. *Mater. Today Energy* **2018**, *9*, 198–222.

(2)   Huskić, I.; Friščić, T. Geomimetic Approaches in the Design and Synthesis of Metal-Organic Frameworks. *Philos. Trans. Royal Soc. A* **2019**, *377* (2149).

(3)   Thorarinsdottir, A. E.; Harris, T. D. Metal-Organic Framework Magnets. *Chem. Rev.* **2020**, *120* (16), 8716–8789.

(4)   Cui, R.; Li, R.; Li, Z.; Wei, M.; Wang, X.; Li, X. A Tb-MOF Anion, Porous Coordination Framework Constructed with Oxalate Ligand: Crystal Structure, Adsorption Properties, and Luminescence Sensing. *Dye. Pigment.* **2021**, *195* (June), 109669.

(5)   Akhtar, M. N.; Chen, Y.-C.; AlDamen, M. A.; Tong, M.-L. 3D Oxalato-Bridged Lanthanide(III) MOFs with Magnetocaloric, Magnetic and Photoluminescence Properties. *Dalt. Trans.* **2017**, *46* (1), 116–124.

(6)   Liu, C.-M.; Zhang, D.-Q.; Zhu, D.-B. Slow Magnetic Relaxation of a Three-Dimensional Metal–Organic Framework Featuring a Unique Dysprosium(III) Oxalate Layer. *RSC Adv.* **2015**, *5* (78), 63186–63192.

(7)   Sanchez, C.; Shea, K. J.; Kitagawa, S.; Schubert, U. Multifunctionality in Hybrid Magnetic Materials Based on Bimetallic Oxalate Complexes. *Chem. Soc. Rev.* **2011**, *40* (2), 453–1152.

(8)   Abraham, F.; Arab-Chapelet, B.; Rivenet, M.; Tamain, C.; Grandjean, S. Actinide Oxalates, Solid State Structures and Applications. *Coord. Chem. Rev.* **2014**, *266–267* (1), 28–68.

(9)   Baran, E. J. Natural Iron Oxalates and Their Analogous Synthetic Counterparts: A Review. *Geochemistry* **2016**, *76* (3), 449–460.

(10)   Echigo, T.; Kimata, M. Crystal Chemistry and Genesis of Organic Minerals: A Review of Oxalate and Polycyclic Aromatic Hydrocarbon Minerals. *Can. Mineral.* **2010**, *48* (6), 1329–1358.

(11)   Dutton, M. V.; Evans, C. S. Oxalate Production by Fungi: Its Role in Pathogenicity and Ecology in the Soil Environment. *Can. J. Microbiol.* **1996**, *42* (9), 881–895.

(12)   Giordani, P.; Modenesi, P.; Tretiach, M. Determinant Factors for the Formation of the Calcium Oxalate Minerals, Weddellite and Whewellite, on the Surface of Foliose Lichens. *Lichenol.* **2003**, *35* (3), 255–270.

(13)   Coe, F. L.; Evan, A.; Worcester, E. Kidney Stone Disease. *J. Clin. Invest.* **2005**, *115* (10), 2598–2608.

(14)   Khan, S. R.; Pearle, M. S.; Robertson, W. G.; Gambaro, G.; Canales, B. K.; Doizi, S.; Traxer, O.; Tiselius, H.-G. Kidney Stones. *Nat. Rev. Dis. Prim.* **2016**, *2* (1), 16008.

(15)   Daudon, M.; Dessombz, A.; Frochot, V.; Letavernier, E.; Haymann, J.-P.; Jungers, P.; Bazin, D. Comprehensive Morpho-Constitutional Analysis of Urinary Stones Improves Etiological Diagnosis and Therapeutic Strategy of Nephrolithiasis. *Comptes Rendus Chim.* **2016**, *19* (11–12), 1470–1491.

(16)   Van de Perre, E.; Bazin, D.; Estrade, V.; Bouderlique, E.; Wissing, K. M.; Daudon, M.; Letavernier, E. Randall's Plaque as the Origin of Idiopathic Calcium Oxalate Stone Formation: An Update. *Comptes Rendus. Chim.* **2022**, *25* (S1), 373–391.

(17)   Izatulina, A. R.; Gurzhiy, V. V; Krzhizhanovskaya, M. G.; Kuz'mina, M. A.; Leoni, M.; Frank-Kamenetskaya, O. V. Hydrated Calcium Oxalates: Crystal Structures, Thermal Stability, and

Phase Evolution. *Cryst. Growth Des.* **2018**, *18* (9), 5465–5478.

(18) Hochrein, O.; Thomas, A.; Kniep, R. Revealing the Crystal Structure of Anhydrous Calcium Oxalate, Ca[C$_2$O$_4$], by a Combination of Atomistic Simulation and Rietveld Refinement. *Zeitschrift für Anorg. und Allg. Chemie* **2008**, *634* (11), 1826–1829.

(19) Gehl, A.; Dietzsch, M.; Mondeshki, M.; Bach, S.; Häger, T.; Panthöfer, M.; Barton, B.; Kolb, U.; Tremel, W. Anhydrous Amorphous Calcium Oxalate Nanoparticles from Ionic Liquids: Stable Crystallization Intermediates in the Formation of Whewellite. *Chem. - A Eur. J.* **2015**, *21* (50), 18192–18201.

(20) Shepelenko, M.; Feldman, Y.; Leiserowitz, L.; Kronik, L. Order and Disorder in Calcium Oxalate Monohydrate: Insights from First-Principles Calculations. *Cryst. Growth Des.* **2020**, *20* (2), 858–865.

(21) Begun, G. M.; Fletcher, W. H. Vibrational Spectra of Aqueous Oxalate Ion. *Spectrochim. Acta* **1963**, *19* (8), 1343–1349.

(22) Shippey, T. A. Vibrational Studies of Anhydrous Lithium, Sodium and Potassium Oxalates. *J. Mol. Biol.* **1980**, *67*, 223–233.

(23) Clark, R. J. H.; Firth, S. Raman, Infrared and Force Field Studies of K$_2$^{12}C$_2$O$_4$·H$_2$O and K$_2$^{13}C$_2$O$_4$·H$_2$O in the Solid State and in Aqueous Solution, and of (NH$_4$)$_2$^{12}C$_2$O$_4$·H$_2$O and (NH$_4$)$_2$^{13}C$_2$O$_4$·H$_2$O in the Solid State. *Spectrochim. Acta Part A Mol. Biomol. Spectrosc.* **2002**, *58* (8), 1731–1746.

(24) Frost, R. L.; Weier, M. L. Thermal Treatment of Whewellite - A Thermal Analysis and Raman Spectroscopic Study. *Thermochim. Acta* **2004**, *409* (1), 79–85.

(25) Echigo, T.; Kimata, M. Single-Crystal X-Ray Diffraction and Spectroscopic Studies on Humboldtine and Lindbergite: Weak Jahn–Teller Effect of Fe^{2+} Ion. *Phys. Chem. Miner.* **2008**, *35* (8), 467–475.

(26) Leroy, C. Oxalates de Calcium et Hydroxyapatite: Des Matériaux Synthétiques et Naturels Étudiés Par Techniques RMN et DNP, PhD Thesis, Université Pierre et Marie Curie - Paris VI, 2016.

(27) Lee, M.; Schaumburg, K. Coordination-site Exchange and Solid-state ^{13}C NMR Studies of Bis(Oxalato)Dioxovanadate(V) Ion. *Magn. Reson. Chem.* **1991**, *29* (9), 865–869.

(28) Zhu, J.; Ye, E.; Terskikh, V.; Wu, G. Solid-State ^{17}O NMR Spectroscopy of Large Protein–Ligand Complexes. *Angew. Chemie Int. Ed.* **2010**, *49* (45), 8399–8402.

(29) Kong, X.; Terskikh, V. V.; Khade, R. L.; Yang, L.; Rorick, A.; Zhang, Y.; He, P.; Huang, Y.; Wu, G. Solid-State ^{17}O NMR Spectroscopy of Paramagnetic Coordination Compounds. *Angew. Chemie* **2015**, *127* (16), 4835–4839.

(30) Michaelis, V. K.; Keeler, E. G.; Ong, T.-C.; Craigen, K. N.; Penzel, S.; Wren, J. E. C.; Kroeker, S.; Griffin, R. G. Structural Insights into Bound Water in Crystalline Amino Acids: Experimental and Theoretical ^{17}O NMR. *J. Phys. Chem. B* **2015**, *119* (25), 8024–8036.

(31) Wong, A.; Pike, K. J.; Jenkins, R.; Clarkson, G. J.; Anupõld, T.; Howes, A. P.; Crout, D. H. G.; Samoson, A.; Dupree, R.; Smith, M. E. Experimental and Theoretical ^{17}O NMR Study of the Influence of Hydrogen-Bonding on CO and O−H Oxygens in Carboxylic Solids. *J. Phys. Chem. A* **2006**, *110* (5), 1824–1835.

(32) Wong, A.; Poli, F. *Solid-State ^{17}O NMR Studies of Biomolecules*, 1st ed.; Elsevier Ltd., 2014; Vol. 83.

(33) Zhao, W.; Sharma, N.; Jones, F.; Raiteri, P.; Gale, J. D.; Demichelis, R. Anhydrous Calcium Oxalate Polymorphism: A Combined Computational and Synchrotron X-Ray Diffraction Study.

Cryst. Growth Des. **2016**, *16* (10), 5954–5965.

(34) Frost, R. L.; Weier, M. L. Thermal Treatment of Weddellite—a Raman and Infrared Emission Spectroscopic Study. *Thermochim. Acta* **2003**, *406* (1–2), 221–232.

(35) Dollimore, D. The Thermal Decomposition of Oxalates. *Thermochim. Acta* **1987**, *117*, 331–363.

(36) Goldberga, I.; Patris, N.; Chen, C.-H.; Thomassot, E.; Trébosc, J.; Hung, I.; Gan, Z.; Berthomieu, D.; Métro, T.-X.; Bonhomme, C.; et al. First Direct Insight into the Local Environment and Dynamics of Water Molecules in the Whewellite Mineral Phase: Mechanochemical Isotopic Enrichment and High-Resolution ^{17}O and ^{2}H NMR Analyses. *J. Phys. Chem. C* **2022**, *126* (29), 12044–12059.

(37) Nour, S.; Widdifield, C. M.; Kobera, L.; Burgess, K. M. N.; Errulat, D.; Terskikh, V. V.; Bryce, D. L. Oxygen-17 NMR Spectroscopy of Water Molecules in Solid Hydrates. *Can. J. Chem.* **2016**, *94* (3), 189–197.

(38) Špačková, J.; Fabra, C.; Cazals, G.; Hubert-Roux, M.; Schmitz-Afonso, I.; Goldberga, I.; Berthomieu, D.; Lebrun, A.; Métro, T.-X.; Laurencin, D. Cost-Efficient and User-Friendly ^{17}O/^{18}O Labeling Procedures of Fatty Acids Using Mechanochemistry. *Chem. Commun.* **2021**, *57* (55), 6812–6815.

(39) Métro, T.-X.; Gervais, C.; Martinez, A.; Bonhomme, C.; Laurencin, D. Unleashing the Potential of ^{17}O NMR Spectroscopy Using Mechanochemistry. *Angew. Chemie Int. Ed.* **2017**, *56* (24), 6803–6807.

(40) Špačková, J.; Goldberga, I.; Yadav, R.; Cazals, G.; Lebrun, A.; Verdié, P.; Métro, T.; Laurencin, D. Fast and Cost-Efficient ^{17}O-Isotopic Labeling of Carboxylic Groups in Biomolecules: From Free Amino Acids to Peptide Chains. *Chem. – A Eur. J.* **2023**, *29* (10).

(41) MassLynx V4.1 https://shorturl.at/DMS78 .

(42) Harris, R. K.; Becker, E. D.; Cabral De Menezes, S. M.; Granger, P.; Hoffman, R. E.; Zilm, K. W. Further Conventions for NMR Shielding and Chemical Shifts (IUPAC Recommendations 2008). *Pure Appl. Chem.* **2008**, *80* (1), 59–84.

(43) Morcombe, C. R.; Zilm, K. W. Chemical Shift Referencing in MAS Solid State NMR. *J. Magn. Reson.* **2003**, *162* (2), 479–486.

(44) Comellas, G.; Lopez, J. J.; Nieuwkoop, A. J.; Lemkau, L. R.; Rienstra, C. M. Straightforward, Effective Calibration of SPINAL-64 Decoupling Results in the Enhancement of Sensitivity and Resolution of Biomolecular Solid-State NMR. *J. Magn. Reson.* **2011**, *209* (2), 131–135.

(45) Fung, B. M.; Khitrin, A. K.; Ermolaev, K. An Improved Broadband Decoupling Sequence for Liquid Crystals and Solids. *J. Magn. Reson.* **2000**, *101*, 97–101.

(46) Fernandez, C.; Lang, D. P.; Amoureux, J. P.; Pruski, M. Measurement of Heteronuclear Dipolar Interactions between Quadrupolar and Spin-1/2 Nuclei in Solids by Multiple-Quantum REDOR NMR. *J. Am. Chem. Soc.* **1998**, *120* (11), 2672–2673.

(47) Gan, Z.; Hung, I.; Wang, X.; Paulino, J.; Wu, G.; Litvak, I. M.; Gor'kov, P. L.; Brey, W. W.; Lendi, P.; Schiano, J. L.; et al. NMR Spectroscopy up to 35.2 T Using a Series-Connected Hybrid Magnet. *J. Magn. Reson.* **2017**, *284*, 125–136.

(48) Amoureux, J.-P.; Fernandez, C. Triple, Quintuple and Higher Order Multiple Quantum MAS NMR of Quadrupolar Nuclei. *Solid State Nucl. Magn. Reson.* **1998**, *10* (4), 211–223.

(49) Cadars, S.; Sein, J.; Duma, L.; Lesage, A.; Pham, T. N.; Baltisberger, J. H.; Brown, S. P.; Emsley, L. The Refocused INADEQUATE MAS NMR Experiment in Multiple Spin-Systems: Interpreting Observed Correlation Peaks and Optimising Lineshapes. *J. Magn. Reson.* **2007**, *188* (1), 24–34.

(50) Martineau, C.; Bouchevreau, B.; Taulelle, F.; Trébosc, J.; Lafon, O.; Paul Amoureux, J. High-Resolution through-Space Correlations between Spin-1/2 and Half-Integer Quadrupolar Nuclei Using the MQ-D-R-INEPT NMR Experiment. *Phys. Chem. Chem. Phys.* **2012**, *14* (19), 7112.

(51) Brinkmann, A.; Kentgens, A. P. M. Proton-Selective ^{17}O−H Distance Measurements in Fast Magic-Angle-Spinning Solid-State NMR Spectroscopy for the Determination of Hydrogen Bond Lengths. *J. Am. Chem. Soc.* **2006**, *128* (46), 14758–14759.

(52) Rakhmatullin, A.; Šimko, F.; Véron, E.; Allix, M.; Martineau-Corcos, C.; Fitch, A.; Fayon, F.; Shakhovoy, R. A.; Okhotnikov, K.; Sarou-Kanian, V.; et al. X-Ray Diffraction, NMR Studies, and DFT Calculations of the Room and High Temperature Structures of Rubidium Cryolite, Rb_3AlF_6. *Inorg. Chem.* **2020**, *59* (9), 6308–6318.

(53) Thurber, K. R.; Tycko, R. Measurement of Sample Temperatures under Magic-Angle Spinning from the Chemical Shift and Spin-Lattice Relaxation Rate of ^{79}Br in KBr Powder. *J. Magn. Reson.* **2009**, *196* (1), 84–87.

(54) Daudon, M.; Bazin, D.; André, G.; Jungers, P.; Cousson, A.; Chevallier, P.; Véron, E.; Matzen, G. Examination of Whewellite Kidney Stones by Scanning Electron Microscopy and Powder Neutron Diffraction Techniques. *J. Appl. Crystallogr.* **2009**, *42* (1), 109–115.

(55) Kresse, G.; Furthmüller, J. Efficiency of Ab-Initio Total Energy Calculations for Metals and Semiconductors Using a Plane-Wave Basis Set. *Comput. Mater. Sci.* **1996**, *6* (1), 15–50.

(56) Kresse, G.; Hafner, J. Ab Initio Molecular Dynamics for Liquid Metals. *Phys. Rev. B* **1993**, *47* (1), 558–561.

(57) Giannozzi, P.; Baroni, S.; Bonini, N.; Calandra, M.; Car, R.; Cavazzoni, C.; Ceresoli, D.; Chiarotti, G. L.; Cococcioni, M.; Dabo, I.; et al. QUANTUM ESPRESSO: A Modular and Open-Source Software Project for Quantum Simulations of Materials. *J. Phys. Condens. Matter* **2009**, *21* (39), 395502.

(58) Perdew, J. P.; Burke, K.; Ernzerhof, M. Generalized Gradient Approximation Made Simple. *Phys. Rev. Lett.* **1996**, *77* (18), 3865–3868.

(59) Troullier, N.; Martins, J. L. Efficient Pseudopotentials for Plane-Wave Calculations. *Phys. Rev. B* **1991**, *43* (3), 1993–2006.

(60) Bylander, D. M.; Kleinman, L. Efficacious Form for Model Pseudopotentials. *Phys. Rev. Lett.* **1982**, *48* (20), 1425–1428.

(61) Pickard, C. J.; Mauri, F. All-Electron Magnetic Response with Pseudopotentials: NMR Chemical Shifts. *Phys. Rev. B* **2001**, *63* (24), 245101.

(62) Kutzelnigg, W.; Fleischer, U.; Schindler, M. The IGLO-Method: Ab-Initio Calculation and Interpretation of NMR Chemical Shifts and Magnetic Susceptibilities. In *Deuterium and Shift Calculation*; 1991; pp 165–262.

(63) Profeta, M.; Benoit, M.; Mauri, F.; Pickard, C. J. First-Principles Calculation of the 17 O NMR Parameters in Ca Oxide and Ca Aluminosilicates: The Partially Covalent Nature of the Ca−O Bond, a Challenge for Density Functional Theory. *J. Am. Chem. Soc.* **2004**, *126* (39), 12628–12635.

(64) Wong, A.; Thurgood, G.; Dupree, R.; Smith, M. E. A First-Principles Computational ^{17}O NMR Investigation of Metal Ion–Oxygen Interactions in Carboxylate Oxygens of Alkali Oxalates. *Chem. Phys.* **2007**, *337* (1–3), 144–150.

(65) Pyykkö, P. Year-2017 Nuclear Quadrupole Moments. *Mol. Phys.* **2018**, *116* (10), 1328–1338.

(66) Herzfeld, J.; Berger, A. E. Sideband Intensities in NMR Spectra of Samples Spinning at the Magic Angle. *J. Chem. Phys.* **1980**, *73* (12), 6021–6030.

(67)   VandeVondele, J.; Krack, M.; Mohamed, F.; Parrinello, M.; Chassaing, T.; Hutter, J. Quickstep: Fast and Accurate Density Functional Calculations Using a Mixed Gaussian and Plane Waves Approach. *Comput. Phys. Commun.* **2005**, *167* (2), 103–128.

(68)   Grimme, S.; Antony, J.; Ehrlich, S.; Krieg, H. A Consistent and Accurate Ab Initio Parametrization of Density Functional Dispersion Correction (DFT-D) for the 94 Elements H-Pu. *J. Chem. Phys.* **2010**, *132* (15).

(69)   Goedecker, S.; Teter, M.; Hutter, J. Separable Dual-Space Gaussian Pseudopotentials. *Phys. Rev. B* **1996**, *54* (3), 1703–1710.

(70)   VandeVondele, J.; Hutter, J. Gaussian Basis Sets for Accurate Calculations on Molecular Systems in Gas and Condensed Phases. *J. Chem. Phys.* **2007**, *127* (11).

(71)   van Meerten, S. G. J.; Franssen, W. M. J.; Kentgens, A. P. M. SsNake: A Cross-Platform Open-Source NMR Data Processing and Fitting Application. *J. Magn. Reson.* **2019**, *301*, 56–66.

(72)   The Math Works, Inc. MATLAB, version 2021b. https://www.mathworks.com/.

(73)   Colas, H.; Bonhomme-Coury, L.; Diogo, C. C.; Tielens, F.; Babonneau, F.; Gervais, C.; Bazin, D.; Laurencin, D.; Smith, M. E.; Hanna, J. V.; et al. Whewellite, $CaC_2O_4 \cdot H_2O$: Structural Study by a Combined NMR, Crystallography and Modelling Approach. *CrystEngComm* **2013**, *15* (43), 8840.

(74)   Leroy, C.; Bonhomme-Coury, L.; Gervais, C.; Tielens, F.; Babonneau, F.; Daudon, M.; Bazin, D.; Letavernier, E.; Laurencin, D.; Iuga, D.; et al. A Novel Multinuclear Solid-State NMR Approach for the Characterization of Kidney Stones. *Magn. Reson.* **2021**, *2* (2), 653–671.

(75)   Keeler, E. G.; Michaelis, V. K.; Griffin, R. G. ^{17}O NMR Investigation of Water Structure and Dynamics. *J. Phys. Chem. B* **2016**, *120* (32), 7851–7858.

(76)   Keeler, E. G.; Michaelis, V. K.; Wilson, C. B.; Hung, I.; Wang, X.; Gan, Z.; Griffin, R. G. High-Resolution ^{17}O NMR Spectroscopy of Structural Water. *J. Phys. Chem. B* **2019**, *123* (14), 3061–3067.

(77)   Shepelenko, M.; Feldman, Y.; Leiserowitz, L.; Kronik, L. Order and Disorder in Calcium Oxalate Monohydrate: Insights from First-Principles Calculations. *Cryst. Growth Des.* **2020**, *20* (2), 858–865.

(78)   Mazurek, A. H.; Szeleszczuk, Ł.; Pisklak, D. M. A Review on Combination of Ab Initio Molecular Dynamics and NMR Parameters Calculations. *Int. J. Mol. Sci.* **2021**, *22* (9), 4378.

(79)   Palatinus, L.; van der Lee, A. Symmetry Determination Following Structure Solution in P*1*. *J. Appl. Crystallogr.* **2008**, *41* (6), 975–984.

(80)   Zhu, J.; Wu, G. Quadrupole Central Transition ^{17}O NMR Spectroscopy of Biological Macromolecules in Aqueous Solution, *J. Am. Chem. Soc.* **2011**, *133* (4), 920–932.

(81)   Zhu, J.; Kwan, I. C. M.; Wu, G. Quadrupole-Central-Transition ^{17}O NMR Spectroscopy of Protein-Ligand Complexes in Solution, *J. Am. Chem. Soc.* **2009**, *131* (40), 14206–14207.

(82)   Goldberga, I.; Hung, I.; Sarou-Kanian, V.; Gervais, C.; Gan, Z.; Novák-Špačková, J.; Métro, T.-X.; Leroy, C.; Berthomieu, D.; van der Lee, A.; Bonhomme, C.; Laurencin, D. *ChemRxiv* **2024**, DOI: 10.26434/chemrxiv-2024-rtx53-v2. (accessed March 20th 2024).